BRNO UNIVERSITY OF TECHNOLOGY
VYSOKÉ UČENÍ TECHNICKÉ V BRNĚ

FACULTY OF MECHANICAL ENGINEERING
FAKULTA STROJNÍHO INŽENÝRSTVÍ

INSTITUTE OF PHYSICAL ENGINEERING
ÚSTAV FYZIKÁLNÍHO INŽENÝRSTVÍ

CORRELATION AND SPIRAL MICROSCOPY USING A SPATIAL LIGHT MODULATION
KORELAČNÍ A SPIRÁLNÍ MIKROSKOPIE S PROSTOROVOU MODULACÍ SVĚTLA

SHORT VERSION OF DOCTORAL THESIS
ZKRÁCENÁ VERZE DIZERTAČNÍ PRÁCE

AUTHOR — Ing. Petr Bouchal
AUTOR PRÁCE

SUPERVISOR — prof. RNDr. Jiří Petráček, Dr.
ŠKOLITEL

BRNO 2016

Abstract

The doctoral thesis presents a review of the main research results obtained in the course of doctoral studies. In the introductory part, the motivation and technical support for the planned research are discussed in connection with research activities of the group of Experimental Biophotonics at the Institute of Physical Engineering, Brno University of Technology.

The scientific part of the doctoral thesis is divided into two main parts devoted to new imaging concepts and modifications of current experiments to extend their application potential. Achieved results support the research development in the areas of correlation and spiral microscopy, utilizing a spatial light modulation as a key experimental technique. Among the new imaging concepts, the correlation imaging is examined under conditions of partial spatial and temporal coherence of light. Subsequently, the principles of singular optics and nondiffracting propagation of light are advantageously implemented in correlation, holographic and optical microscopy, resulting in advanced imaging techniques and holographic reconstructions. Specifically, the vortex and nondiffracting beams and the self-imaging effects are successfully deployed using either optical or digital tools and gradually applied to 3D spiral imaging ensuring the edge contrast enhancement or axial localization of microobjects by the rotating point spread function. The results obtained by the theoretical analysis and the experimental testing of the proposed imaging modalities are also presented.

In the technical part of the doctoral thesis, up-to-date imaging configurations aided by a spatial light modulator are optimized, allowing the wide-field correlation imaging and achromatic high-resolution imaging by a programmable diffractive lens. In the correlation imaging, the enhanced field of view is achieved by deploying a relay optical system in standard experiments, while achromatic correction of diffractive lenses is implemented by a specially designed refractive corrector. Using birefringence of liquid crystal molecules of light modulating devices, a new phase-shifting technique is proposed and tested in polarization adapted Mirau interferometer. Acquired experimental know-how is fully exploited in the design of multimodal microscope working with different imaging modes implemented using an add-on module connected to standard microscope.

Abstrakt

Dizertační práce je uceleným shrnutím výsledků dosažených v průběhu doktorského studia. V úvodní části práce je představena motivace, odborné a technické zázemí a grantová podpora realizovaného výzkumu. Popsány jsou také dosažené výsledky a jejich význam pro skupinu Experimentální biofotoniky, Ústavu fyzikálního inženýrství, Vysokého učení technického v Brně.

Vědecká část práce je rozdělena do dvou hlavních bloků, které se postupně zabývají návrhem nových zobrazovacích koncepcí a technickou modifikací stávajících zobrazovacích systému v praktických aplikacích. Dosažené vědecké výsledky podporují vývoj v oblastech korelační a spirální mikroskopie s prostorovou modulací světla.

V části zabývající se návrhem nových zobrazovacích koncepcí je provedena studie korelačního zobrazení v podmínkách proměnné časové a prostorové koherence. Následně jsou zkoumány možnosti praktického využití vírových a nedifrakčních svazků v oblastech korelační, holografické a optické mikroskopie. Interference vírových svazků a samozobrazení nedifrakčních svazků je postupně využito k dosažení 3D zobrazení s hranovým kontrastem a rotující bodovou rozptylovou funkcí. Pokročilé zobrazovací metody jsou úspěšně zavedeny optickou cestou ale i digitální modifikací holografických záznamů. Výsledky teoretických modelů a numerických simulací jsou doprovázeny praktickým vyhodnocením navržených zobrazovacích principů.

V technicky zaměřené části jsou navrženy nové způsoby zavedení prostorové modulace světla, které umožňují rozšíření zorného pole v experimentech korelačního zobrazení a dosažení achromatizace při zobrazení pomocí programovatelných difraktivních prvků. Rozšíření zorného pole v korelačních experimentech umožňuje přizpůsobovací optický systém vložený do standardní zobrazovací sestavy. Achromatizace difraktivního zobrazení je zajištěna použitím speciálně navrženého refraktivního korektoru. V navazující části je navržena nová metoda krokování fáze, která pracuje s dvojlomností kapalných krystalů využívaných v systémech pro prostorovou modulaci světla. Použití metody je experimentálně demonstrováno v polarizačně modifikovaném Mirau interferometru. Získané technické zkušenosti jsou využity v praktickém návrhu a realizaci multimodálního zobrazovacího systému s prostorovou modulací světla.

Keywords

digital holography, correlation and spiral microscopy, spatial light modulation, vortex and nondiffracting beams, three-dimensional and quantitative imaging

Klíčová slova

digitální holografie, korelační a spirální mikroskopie, prostorová modulace světla, vírové a nedifrakční svazky, trojrozměrné a kvantitativní zobrazení

Bibliographic citation

BOUCHAL, P. *Correlation and spiral microscopy using a spatial light modulation.* Brno: Brno University of Technology, Faculty of Mechanical Engineering, 1–46, 2016. Supervisor: prof. RNDr. Jiří Petráček, Dr.

I declare that this thesis has been composed by myself under the guidance of my supervisor and that it has not been submitted, in whole or in part, in any previous application for a degree. Any secondary sources and contributions from colleagues in the collaboration are explicitly referenced in the text.

. . . . . .
Petr Bouchal

Acknowledgements

I would like to thank my supervisor, prof. RNDr. Jiří Petráček, Dr., for the guidance he has provided during my doctoral studies. I would also like to thank prof. RNDr. Radim Chmelík, Ph.D., head of the group of Experimental Biophotonics, for his advice, securing funding projects and creating a friendly workplace.

My thanks go also to members of the group of Experimental Biophotonics and colleagues from Department of Optics, Palacky University Olomouc, including my father, prof. RNDr. Zdeněk Bouchal, Dr. He has always been a source of inspiration to me and I have enjoyed working with him on joint projects. Last but not least, I would like to thank my family, girlfriend and friends for all the indisputable support and help.

Contents

1 Topics and meaning of the doctoral thesis **1**

2 Objectives and main outcomes **3**

3 Theoretical and experimental methods and laboratory equipment **5**

4 Outcomes of basic research **7**
4.1 Incoherent correlation imaging 7
4.1.1 Superresolution in monochromatic incoherent correlation imaging . 11
4.1.2 Broadband incoherent correlation imaging 13
4.2 Spiral and Bessel beam imaging 14
4.2.1 Edge enhancement in spiral correlation imaging 15
4.2.2 Axial localization by rotating Bessel beams 17

5 Outcomes of applied research **25**
5.1 Incoherent correlation imaging with extended field of view 25
5.2 Correction of diffractive dispersion in broadband SLM imaging 27
5.3 Polarization adapted Mirau interferometry with liquid crystal variable retarder 29
5.4 Multimodal microscope aided by spatial light modulation 32
5.4.1 Early experimental testing 32

6 Conclusion **37**

Abbreviations **39**

References **41**

Curriculum vitae **45**

1. Topics and meaning of the doctoral thesis

The doctoral thesis is focused on advanced imaging techniques that connect theoretical concepts of traditional and modern optics with methods of digital signal processing and optoelectronic light shaping technologies. The developed imaging techniques are based on the principles of diffractive optics, Fourier optics and digital holography, which are further supported by nondiffracting and self-imaging phenomena [1–3] and recent discoveries in singular optics [4]. The proposed and realized imaging methods operate with the intentionally created nondiffracting and vortex beams enabling specific experiments on image contrast enhancement, quantitative phase imaging or axial localization of microobjects. As a basic experimental tool, a liquid crystal on silicon Spatial Light Modulator (SLM) has been used to create the special states of light and to modify the spatial spectrum of optical signal. The doctoral thesis has been built on the foundations previously established in the bachelor and diploma thesis [5,6]. Its main goal is to deepen the theoretical and experimental background of the SLM aided imaging and to propose original applications of the SLM technology in fluorescence microscopy, spiral microscopy, incoherent correlation holography, quantitative phase imaging and 3D localization of microscopic objects.

The topics developed in the doctoral thesis are closely related to the traditional research established at the Institute of Physical Engineering, the Faculty of Mechanical Engineering, Brno University of Technology (IPE BUT). Specifically, the experiments realized in the doctoral thesis provide support and new ideas for Coherence Controlled Holographic Microscopy (CCHM) [7], that has been invented at the IPE BUT and its applications have permanently emerged at the forefront of a systematic biomedical research [8–10]. When implementing novel experiments of the SLM aided microscopy, an effective cooperation between the IPE BUT and the Department of Optics of the Palacky University in Olomouc (UP) has been established, benefiting from specific know-how of both institutions developed in the fields of holographic microscopy and light shaping technology, respectively. Topicality and interdisciplinary impact of the SLM imaging initiated a joint research programme of both institutions, which became a part of the Center of Digital Optics (CDO) supported by the Technology Agency of the Czech Republic (TA CR). The CDO has been established for a period of eight years and currently it represents a well–functioning Center of excellence with the participation of two academic institutions (IPE BUT and UP) and three major companies operating in the area of Moravia (Meopta-optika, s.r.o., PRAMACOM-HT, s r.o. and ZEBR, s.r.o.). The methods developed throughout the doctoral thesis formed a basis for one of four CDO working packages, called *"Imaging supported by a spatial light modulation."* Outcomes of the doctoral thesis were used not only in the applied research but they also positively influenced a cooperation of the IPE BUT and the UP in the field of basic research. The research activities resulted in the joint project *"Advances in incoherent holographic microscopy using photonic modeling and principles of singular optics"*, supported by the Grant Agency of the Czech Republic (GA CR). Receiving support from the projects of TA CR and GA CR, a new laboratory has been equipped at the IPE BUT, allowing for the cutting-edge experiments in the field of SLM microscopy [11].

2. Objectives and main outcomes

The doctoral thesis is focused on the advanced imaging methods benefiting from connections between recent discoveries of modern optics and sophisticated techniques for light shaping and signal processing. Due to the ongoing technological progress, a powerful experimental background has been created in the SLM aided digital imaging, that has opened new pathways for systematic research with a wide range of applications. The predetermined research plans of the doctoral thesis can be specified as follows:

- Creation of computational models of the incoherent correlation holography describing a two-step image formation and allowing to examine an influence of the partial temporal coherence of light and the diffractive dispersion.
- Design and implementation of the original experimental configurations for the SLM aided common-path interferometry, working with both coherent and spatially incoherent light.
- Incorporation of nondiffracting and vortex beams, self-imaging phenomena and principles of singular optics into the advanced imaging techniques of optical microscopy and digital holography.
- Implementation of new experiments of the quantitative phase imaging using the SLM as an active element and the development of efficient techniques for the Point Spread Function (PSF) engineering.
- Optimization of the developed imaging techniques to design the functional prototype of a versatile microscope implemented by commercially available and customized optical components.

The doctoral thesis succeeded in meeting the challenges outlined and the original concepts and experiments for the SLM aided imaging were designed and implemented. The functionality of the experiments was systematically examined using appropriate testing objects, such as resolution targets, fluorescent and transparent specimens, polystyrene beads or calibration reflective surfaces for phase reconstruction techniques. To optimize operation of the proposed experiments, significant technical improvements were realized, providing an increased optical performance. Technical modifications of experiments with major benefits for applications can be summarized as follows:

- The basic setup for the incoherent correlation holography was supplemented by relay lenses to eliminate a spatial separation of signal and reference waves during the free space propagation towards the CCD. By the relay lenses, a perfect overlapping of the interfering waves was ensured in the entire field of view of the used microscope objective [12].
- A refractive afocal optical system was designed and manufactured in Meopta-optika, s.r.o., enabling an achromatic correction of a diffractive dispersion of the SLM in imaging applications [13]. Both a utility model and a patent were applied to protect the design of the afocal dispersion corrector [14].

- A significant technical simplification of the experiments enabling an axial localization of microparticles by rotating vortex structures was proposed and verified. In the enhanced setup, a spiral phase modulation generating optical vortices is implemented by specially designed diffractive masks. Production of the spiral masks was carried out in a cooperation with the Institute of Scientific Instruments Brno (ISI Brno) by electron beam lithography.

- The custom polarization modification of a commercial Mirau interference objective was proposed to realize a polarization sensitive phase-shifting by a Liquid Crystal Variable Retarder (LCVR). Using this technique, an original setup enabling the quantitative phase imaging with a nanometer precision was implemented [15].

- The functional prototype of multimodal SLM aided microscope was built and its early experimental testing was performed, providing promising results for ongoing basic and applied research.

The most important results of the doctoral thesis were published in the prestigious physical and optical journals (New Journal of Physics IF 3.558, 1×, [16]; Optics Express, IF 3.488, 4×, [13,17–19]; Optics Letters IF 3.292, 2×, [15,20]; Journal of the European Optical Society–Rapid Publications IF 1.231, 1×, [12]), presented at the international conferences (poster presentations 3×, oral presentation 1×) and the workshops of the CDO TA CR (oral presentations 3x). The results of the doctoral thesis were used as the basis of a comprehensive research report summarizing the activities of the Work Package No. 4 of the CDO TA CR (60 pages, [21]). The results of the doctoral thesis also contributed to the presentation of the IPE BUT in 2 papers published in Czech journals (*"Jemná mechanika a optika"* [11] and *"Československý časopis pro fyziku"* [22]). Activities of the doctoral thesis have also contributed to the preparation of the utility model and Czech and European patent applications, which were submitted in 2015 and 2016, respectively [14].

3. Theoretical and experimental methods and laboratory equipment

The doctoral thesis is focused on advanced imaging methods profiting from recent discoveries of singular, diffractive and digital optics and utilizing versatile technologies for light shaping. Basic theoretical background of the doctoral thesis has been created by a systematic study of scientific publications in relevant areas of optics. In subsequent research, the original imaging techniques were developed and the improvements of some up-to-date experiments proposed. As basic tools of the theoretical research, both accurate and approximate computational models were used, supplemented by numerical simulations preferably prepared in Matlab. In a direct contact with the experiments, digital techniques were elaborated, enabling the control of optoelectronic devices and measurement processes. The control of some peripheral units was ensured through a LabView interface or using a commercial software. A special attention was also paid to the numerical methods for signal processing and digital image reconstruction applied to experimental data acquired in the setups for correlation holography or quantitative phase imaging.

The experiments were carried out in a new laboratory established at the IPE BUT, which was equipped under the support of GA CR and TA CR projects. Due to a close collaboration between the IPE BUT and the UP, the Laboratory of digital optics (Department of Optics, UP in Olomouc) [23] was available for experiments of the doctoral thesis, which were involved in the scientific program of the joint GA CR and TA CR projects. As a key technology constituting the basis of almost all experiments, a spatial light modulation was used. Due to a complexity of operation, the SLM was deployed almost exclusively in the doctoral thesis [24,25]. In the experiments based on a polarization sensitive phase-shifting, the LCVRs Thorlabs and Arcoptix providing a constant phase retardation were successfully used [26,27].

In imaging applications requiring a spatially variable phase modulation, the reflective SLM Hamamatsu X10468-01, operating in a phase-only mode, was utilized [25]. These devices are available in both the IPE BUT and the UP laboratories. To control the SLM effectively, techniques for making Computer Generated Holograms (CGHs) have been developed as a part of the doctoral thesis. The CGH represents a bitmap, which is encoded into the electric signals and transferred from the PC to the active display of the SLM. In the implemented experiments, the SLM was controlled by the CGHs created in Matlab, using principles of diffractive, Fourier and singular optics. In some cases, a complex modulation, involving both amplitude and phase changes of light, was required. Performing the precisely controlled complex modulation of light by means of a phase-only SLM is difficult. To achieve it, special iterative algorithms for the CGH generation were used, or alternatively, a phase-only modulation was combined with a spatial filtering of light in the Fourier domain.

4. Outcomes of basic research

The doctoral thesis is divided into parts devoted to basic and applied research, where the achieved results and activities are discussed separately.

The main outputs of basic research were obtained by examining new principles of incoherent correlation holography and digital holographic microscopy. The examined techniques of digital imaging can be considered as a two-stage process. Acquisition of experimental data performed in the optical stage is followed by the signal processing and digital image reconstruction. Using a SLM during the data acquisition, imaging variability was significantly enhanced. It allowed multitude of imaging modes, which were introduced either optically or digitally. The proposed and experimentally tested imaging modes are summarized in Fig. 1.

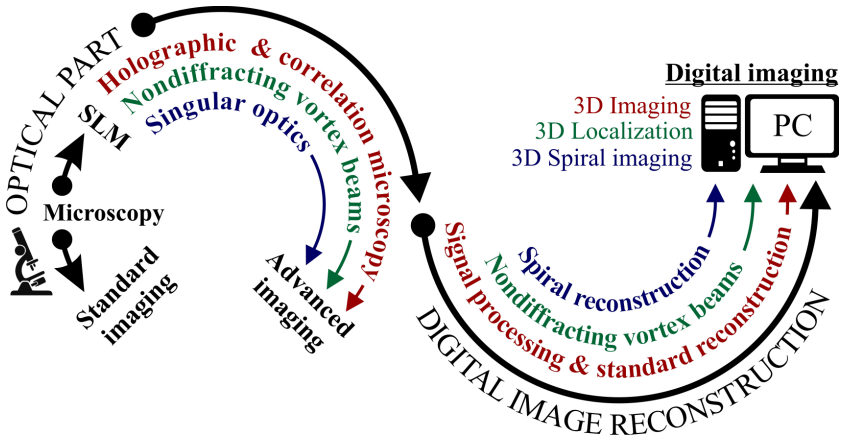

Figure 1: Imaging modes available in the SLM aided incoherent correlation holography and digital holographic microscopy. Variability of imaging is achieved by versatile light shaping and advanced data processing carried out in optical and digital parts of the developed methods.

In basic configurations, the SLM was used as a tube lens with a variable focal length. It enabled adaptive refocusing in a conventional bright-field microscope. The bright-field microscope can be advantageously transformed into a common-path interferometer provided the SLM is operated as a diffractive beam-splitting and phase-shifting device. By dividing each incident wave into two spatially coherent waves, experiments of correlation imaging and incoherent holographic microscopy were introduced. Principles of singular optics were transferred into the correlation imaging either by optical or digital modifications of the basic experiment. The proposed spiral correlation imaging provided anisotropic edge contrast enhancement of three-dimensional objects. The self-imaging of nondiffracting vortex beams was successfully deployed in a Double-Helix Point Spread Function (DH PSF) engineering allowing a three-dimensional localization of microparticles in optical microscopy, digital holography and incoherent correlation imaging.

4.1. Incoherent correlation imaging

Incoherent correlation microscopy is based on a new method of digital imaging using holograms recorded under spatially incoherent illumination, that maintains either nearly perfect or reduced temporal coherence [28,29]. The incoherent correlation imaging effectively combines optical microscopy and exceptionally stable common-path interferometry with

digital signal processing and numerical image reconstruction. In a basic experimental configuration, the SLM is placed at the output of a standard microscope, where interfering waves are created by various methods of diffractive [20,28,30] or birefringent beam splitting [31]. At the CCD, the interference records of individual points of a three-dimensional sample are captured simultaneously and reconstructed numerically adopting methods known from digital holography.

The correlation imaging is based on the fact that every point source, either scattering or emitting light, is spatially self-coherent. In the imaging process, light scattered or emitted by the sample is captured by an optical system and directed towards the SLM. Waves emanating from the individual object points are divided by the SLM to pairs of signal and reference waves, creating interference patterns representing point holographic records. Because light from different points of the object is not correlated, the record of the entire three-dimensional object is created as an incoherent superposition of the individual point holograms. The correlation imaging works in a common-path configuration that provides exceptional vibration resistance and minimal optical path difference of interfering waves. On the other hand, faithful image reconstruction is not possible with a single holographic exposure and both DC term and twin-image have to be eliminated by the phase-shifting technique requiring multiple recordings of the object [28,32]. From at least three records processed by the phase-shifting, three-dimensional amplitude objects can be numerically reconstructed. Optical performance of the image reconstruction strongly depends on the configuration and parameters of the experiment and temporal coherence of light (Fig. 2).

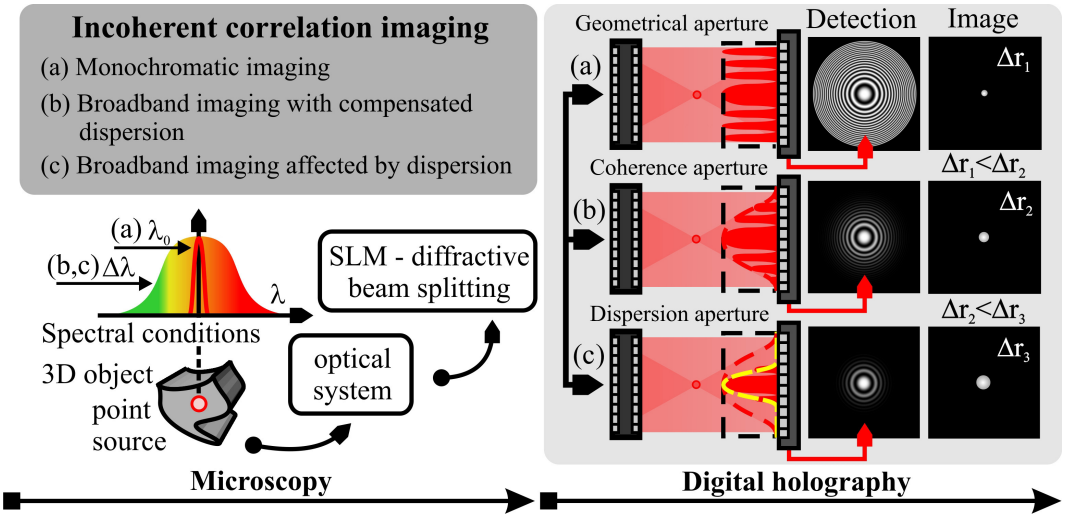

Figure 2: Schema of incoherent correlation microscopy with point holographic records and reconstructed images obtained under different spectral conditions: (a) geometrical aperture-monochromatic illumination, (b) coherence aperture-broadband illumination in dispersion-free system, (c) dispersion aperture-broadband illumination in system with diffractive dispersion.

In the incoherent correlation imaging, the entire record of a three-dimensional object is composed of an infinite number of point holograms superimposed incoherently. The image quality can be assessed using the PSF obtained by the reconstruction of a single point hologram. As the point hologram is created by signal and reference waves originating from the same point source, a full spatial coherence is inherently ensured. The interference of

waves is still significantly affected by the temporal coherence of light determined by the spectral properties of the source. Under conditions of partial temporal coherence of light, the intensity of the point correlation record is obtained by the time averaging,

$$I_j = \langle |U_s(t)\exp(i\theta_j) + U_r(t+\tau)|^2 \rangle, \quad j = 1, 2, 3, \tag{1}$$

where t and τ represent a reference time and a time delay, respectively, and $U_m \equiv U_m(\mathbf{r}_c; \mathbf{r}_0, t), m = s, r$, denote the random complex amplitudes of the signal and reference waves. They depend on the vectors $\mathbf{r}_0$ and $\mathbf{r}_c$ determining positions of the recorded object point and the points of the CCD, respectively. The correlation records are carried out for three different phase shifts $\theta_1 = 0$, $\theta_2 = 2\pi/3$ and $\theta_3 = 4\pi/3$, imposed on the signal wave. Applying the phase-shifting procedure to the intensity patterns (1), the DC term and the twin image are removed [28,32]. The record to be reconstructed then provides a faithful image and can be written as $H = a_p U_s U_r^*$, where a_p is an aperture function. In the doctoral thesis, both the processed point recording H and the PSF obtained by its reconstruction were described analytically and examined in detail [5,6,18]. In the developed models it has been shown that the recording H can be interpreted as a virtual diffractive lens, whose axis position and the focal length f_d provide information about the lateral and longitudinal position of the recorded point object. To assess the optical performance of the imaging, the aperture function a_p is of a particular importance, because it determines the lateral size and the numerical aperture NA' of the virtual diffractive lens. Calculation of the aperture function a_p and the numerical aperture NA' is challenging in the correlation imaging due to a complicated connection with the parameters of the experiment, spatial overlapping of interfering waves and temporal coherence of light. For this reason, the concepts of the correlation imaging were developed at two different theoretical levels based on the assumption of monochromatic and broadband illumination.

Monochromatic correlation imaging

In the theoretical model of the monochromatic correlation imaging, the spectral width of light $\Delta\lambda = 0$ is assumed. The coherence length $L_c \to \infty$ is then attained and the signal and reference waves can interfere for any optical path difference. The aperture function is then clearly identified as a geometric area created by a spatial overlapping of the signal and reference waves at the detection plane. It depends on the CCD coordinates given by the position vector $\mathbf{r}_c$, $a_p \equiv a_g(\mathbf{r}_c; \mathbf{r}_0)$ (Fig. 2a). In initial experiments, the overlapping area was strongly reduced for off-axis object positions $\mathbf{r}_0$, so that only a very narrow field of view was available in the correlation imaging. In the doctoral thesis, the geometrically defined aperture function was examined by a ray tracing and improved experiments were designed ensuring a perfect overlapping of interfering waves in the entire field of view of the microscope objective [12]. In advanced configurations of monochromatic correlation imaging, both diffraction limited resolution [18] and resolution beyond the diffraction limit were successfully demonstrated [30,33], provided appropriate recording configurations were applied. In the experiments, the conditions of monochromatic spatially incoherent imaging are approximately satisfied only if spectral filters with the bandwidth in units of nanometers are used. Under these conditions, the signal to noise ratio is significantly deteriorated.

Broadband correlation imaging with compensated dispersion

In experiments of the incoherent correlation imaging, fluorescence specimens or objects illuminated by a light emitting diode (LED) are most commonly investigated. In these

cases, the spectral width reaches several tens of nanometers. Such light is regarded as broadband because it causes significant effects related to the partial temporal coherence and the diffractive dispersion. When broadband light is used, the aperture function is no longer clearly determined by the spatial overlapping of interfering waves. The aperture size has a complicated dependence on the temporal coherence of light, the optical path difference and the dispersion, which is dominant when diffractive elements are used. In the doctoral thesis, the broadband correlation imaging was examined both on physical and technical levels. The physical resolution limits were first explored for dispersion-free experiments [16]. Subsequently, an afocal refractive system enabling achromatic correction of the diffractive dispersion was designed, realized and tested in experiments [13,14].

When broadband illumination is used in the dispersion-free experimental systems, the lateral bounding of the point hologram arises due to an interplay of geometric and coherence effects and the aperture function can be written as $a_p = a_g(\mathbf{r}_c;\mathbf{r}_0)a_c(\mathbf{r}_c;\mathbf{r}_0)$. The aperture of the record is then determined as a product of the function a_g corresponding to the geometrical overlapping of interfering waves and the coherence aperture a_c, whose shape depends on the coherence length of light L_c and the optical path difference of the signal and reference waves ΔD [16]. If the spectral width of light or the optical path difference are increased, the coherence aperture becomes more closed and the resolution of the reconstructed image is deteriorated (Fig. 2b). Adopting the concept of the coherence aperture, new experimental configurations with the minimal optical path difference were found, preserving the monochromatic resolution limits even in broadband light [16].

In real experiments of the broadband correlation imaging, a very strong diffractive dispersion of the SLM reduces both the aperture size of the point records and the achievable image resolution. To eliminate unwanted dispersion effects, the experimental configurations with a lower sensitivity to the dispersion were found [16] and the refractive system allowing achromatic correction of the SLM was designed and realized [13]. The correlation imaging working with nearly monochromatic and broadband light was experimentally tested in the setup shown in Fig. 3. The object to be recorded was illuminated by LED, which was combined with narrowband spectral filters when monochromatic imaging was studied. configurations with a lower sensitivity to dispersion were obtained by optimizing the CCD position Δ_2 and the focal lengths f_s and f_r of the lenses displayed on the SLM.

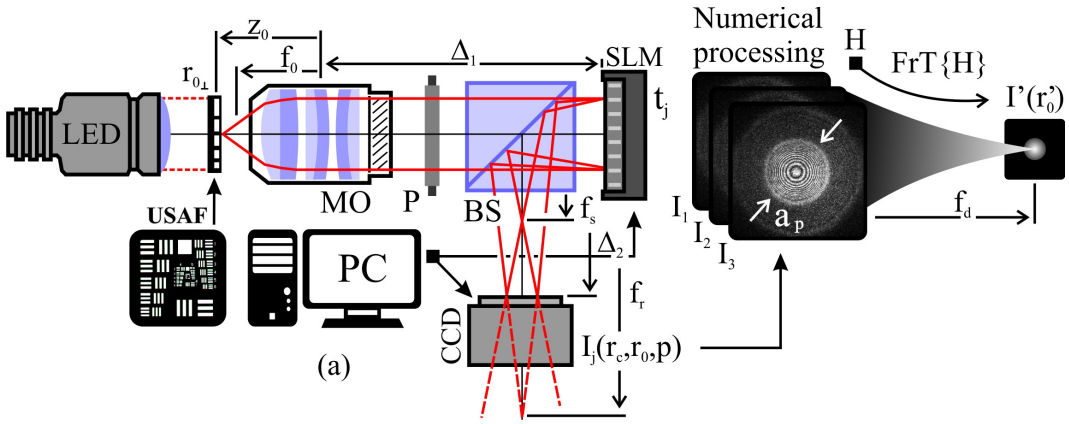

Figure 3: Scheme of incoherent correlation microscopy incorporating both optical and digital stages of imaging process: LED-light emitting diode, MO-microscope objective, P-polarizer, BS-beam splitter, SLM-spatial light modulator, CCD-charged coupled device.

4.1.1. Superresolution in monochromatic incoherent correlation imaging

In conventional optical imaging, the Rayleigh criterion determines the diffraction limit of resolution and the Lagrange invariant can be used to express the lateral magnification as a ratio between the object and image space numerical apertures, $m = NA/NA'$. Applying the Rayleigh criterion to the diffraction limited imaging, two image spots of the same intensity can be regarded as resolved, if the distance of the intensity maxima is equal to the radius of the Airy pattern, $\Delta r' \propto \lambda/NA'$. Since the related distance in the object space is given as $\Delta r = \Delta r'/m = \lambda/NA$, the object space resolution is also diffraction limited. In the incoherent correlation imaging, the Lagrange invariant is not inherently fulfilled and the lateral magnification m can be changed independently from the numerical apertures NA and NA' [18,34,35]. This effect can be used to achieve an optimal image resolution in the incoherent correlation imaging. A violation of the Lagrange invariant can be utilized in two different experimental configurations ensuring that the diffraction resolution limit of the used MO is reached [18] or even exceeded twice [30,33].

In the first superresolving adjustment [33], the violation of the Lagrange invariant was tested for a plane reference wave ($f_r \to \infty$) and a spherical signal wave (f_s). In this configuration, the lateral magnification varies with the CCD position, $m \equiv m(\Delta_2)$, while the image space numerical aperture NA' remains unchanged. It occurs as far as the condition $\Delta_2 \leq 2f_s$ is met [18]. If the lateral magnification $m(\Delta_2)$ and the size of the diffraction image pattern $\Delta r'$ are known, the size of the related object space pattern can be determined as $\Delta r = \Delta r'/m(\Delta_2)$. To quantify a degree of the superresolution, the coefficient $L = \Delta r/\Delta r_0$ may be used, where $\Delta r_0 = \lambda/NA_0$ and NA_0 denotes the numerical aperture of the MO. Dependence of the coefficient L on the ratio Δ_2/f_s is illustrated by the dashed blue line in Fig. 4. As is obvious from Fig. 4, the coefficient $L > 1$ is obtained at the CCD positions $\Delta_2/f_s < 1$. It indicates a deterioration of the resolution of the used MO. At the CCD position $\Delta_2/f_s = 1$, the diffraction limit of the optical imaging is reached and the superresolution is available for $\Delta_2/f_s > 1$. The best resolution is achieved when $\Delta_2/f_s = 2$. In this case the superresolution with factor 2 is reached, meaning that the object space diffraction spot is twice less in the incoherent correlation imaging than in the optical imaging using the MO.

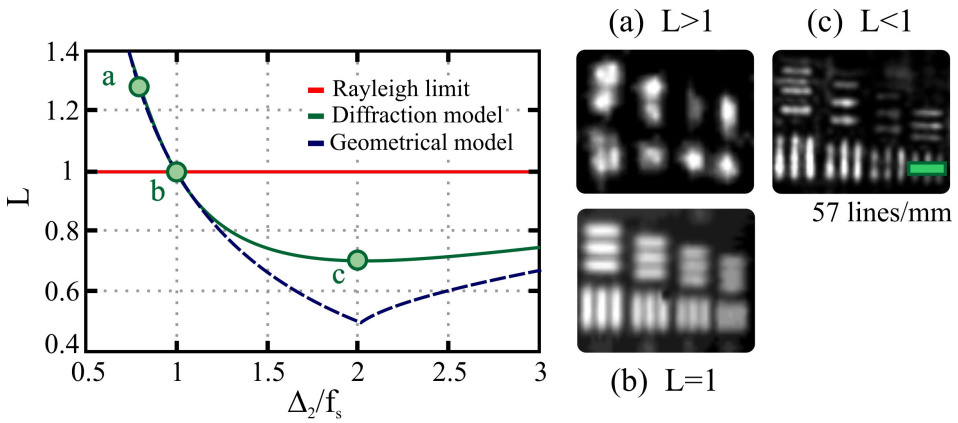

Figure 4: Dependence of the coefficient L on the relative CCD position Δ_2/f_s with areas of the deteriorated imaging ($\Delta_2/f_s < 1$) and the superresolution ($\Delta_2/f_s > 1$). The snapshots (a) and (c) demonstrate degraded and enhanced resolution of the incoherent correlation imaging in comparison with the direct optical imaging (b).

In experiments, the resolution limits were examined using a low magnification MO (achromatic doublet, $NA_0 = 0.15$, $f_0 = 150$ mm). The signal and reference waves were shaped by the diffractive lenses with the focal lengths $f_s = 750$ mm and $f_r \to \infty$, displayed on the SLM. Experimental results obtained with the USAF resolution target are shown in Fig. 4. The images of the resolution target reconstructed from the holograms recorded at the CCD positions $\Delta_2/f_s < 1$ and $\Delta_2/f_s = 2$ are compared with a direct optical image detected at $\Delta_2/f_s = 1$ (points a, b and c on the solid green line in Fig. 4). In the direct imaging, the SLM was used as a tube lens with the focal length $f_s = 750$ mm. As is obvious, the snapshot (c) obtained from the holograms recorded at the optimal CCD position (point c on the solid green line) has apparently higher resolution than the snapshot (b). The practically obtained resolution corresponds to the coefficient $L \approx 1/\sqrt{2}$.

In [30,36], another way of the Lagrange invariant violation was proposed to reach the superresolution. In this method, the spherical signal and reference waves and the CCD position were adapted to each other to achieve the best image resolution, $\Delta_{2opt} = 2f_s f_r/(f_s + f_r)$. The resolution enhancement is then evaluated by the coefficient $M = NA'/NA'_d$, where NA' denotes the numerical aperture of the reconstructed hologram representing a virtual lens with the focal length $f_d = |(\Delta_2 - f_s)(f_r - \Delta_2)|/|f_s - f_r|$ and NA'_d is the image numerical aperture of a conventional imaging system composed of the MO and the tube lens with the focal length equal to Δ_{2opt}. The tube lens is realized by the SLM and its image numerical aperture is given as $NA'_d = R_c/\Delta_{2opt}$, where R_c is the radius of the active area of the SLM. At the CCD positions with $M > 1$, the numerical aperture of the hologram NA' is higher than the numerical aperture of the conventional imaging lens NA'_d and the resolution beyond the diffraction limit is reached. The theoretical dependence of the coefficient M on the relative CCD position Δ_2/Δ_{2opt} is shown in Fig. 5. The CCD setting $\Delta_2/\Delta_{2opt} = 1$ results in $M = 2$ indicating the highest level of the superresolution. The resolution enhancement is the same as in the previously examined case with the plane reference wave [33].

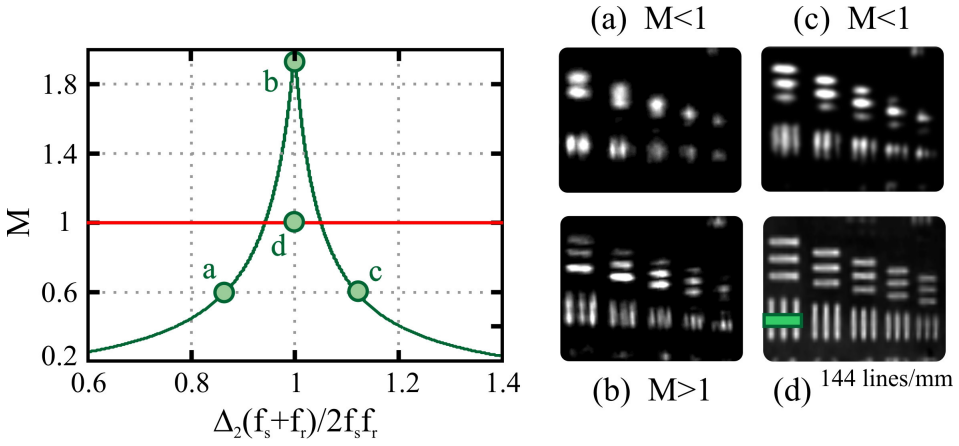

Figure 5: Dependence of the coefficient M on the relative CCD position Δ_2/Δ_{2opt} with indicated superresolution imaging (point b on the green line). The snapshots (a), (b) and (c) reconstructed from the records at the relevant positions of the theoretical green curve do not confirm theoretically predicted resolution enhancement of the optical image created by the MO and the SLM tube lens (snapshot (d)).

In the experiments, the MO Melles Griot ($NA_0 = 0.28$, $f_0 = 20$ mm) and the SLM diffractive lenses with the focal lengths $f_s = 470$ mm and $f_r = 523$ mm were used. The correlation records were captured under system adjustments related to the points a, b and c of the theoretical green curve in Fig. 5. The snapshots (a), (b) and (c) obtained by the numerical reconstruction of the correlation records were compared with the optical image (d), created by the MO and the tube lens displayed on the SLM. In accordance with the theory, the best reconstructed image was obtained in the position b providing the highest numerical aperture NA', but the predicted resolution enhancement of the optical image was not proven. The results of the doctoral thesis indicate that the system working with the spherical reference wave is more sensitive to aberrations, which prevent to achieve superresolution in real experimental conditions. Such problems will be further addressed in subsequent research.

4.1.2. Broadband incoherent correlation imaging

In broadband correlation imaging, the parameters used in monochromatic experiments must be further optimized, in order to achieve a high resolution imaging [16]. This problem was successfully addressed by exploiting the second-order coherence theory in conditions of the correlation imaging. In the proposed model, a close relationship among the temporal coherence of light, the optical path difference of interfering waves and the attainable image resolution was examined and interpreted by original concept of the coherence induced aperture. Within these theoretical concepts, new experiments were designed and tested that enable to reach the monochromatic resolution limits even if a broadband light is used [16,37].

The monochromatic resolution is reached in the broadband correlation imaging provided the coherence aperture a_c is wider than the geometric aperture a_g. Under this condition, the interference pattern representing the point hologram arises in the whole overlapping area of the signal and reference waves and the numerical aperture NA' is not reduced due to a partial temporal coherence of light. Since the width of the coherence aperture a_c depends on both the optical path difference ΔD and the coherence length L_c, the required extension of the aperture can be achieved either by reducing the spectral bandwidth or minimizing ΔD in optimally configured experiments. In real experiments, the width of the aperture of the point holograms is further reduced due to the strong diffractive dispersion of the SLM. To attain a high image resolution, the SLM dispersion must be compensated [13,16] or systems with a reduced sensitivity to the dispersion applied [16].

The results provided by the concept of coherence induced aperture were assessed experimentally in the configurations with a low dispersion sensitivity. In these experiments, the MO Melles Griot ($NA_0 = 0.28$, $f_0 = 20$ mm), the spherical signal wave ($f_s = 400$ mm) and a plane reference wave were used, while the CCD position was varied. The effects caused by the reduced temporal coherence were examined using both the point correlation records and the reconstructions of the USAF resolution target. The experimental results are presented in Fig. 6. The point correlation records captured at the CCD position optimal for monochromatic light ($\Delta_2 = 800$ mm) are shown in Figs. 6a,b. When nearly monochromatic light was used ($\Delta\lambda = 1$ nm), the correlation record with interference oscillations apparent in the entire overlapping area of the signal and reference beams was obtained (area a_g in Fig. 6a). When a broader spectral filter was used ($\Delta\lambda = 20$ nm),

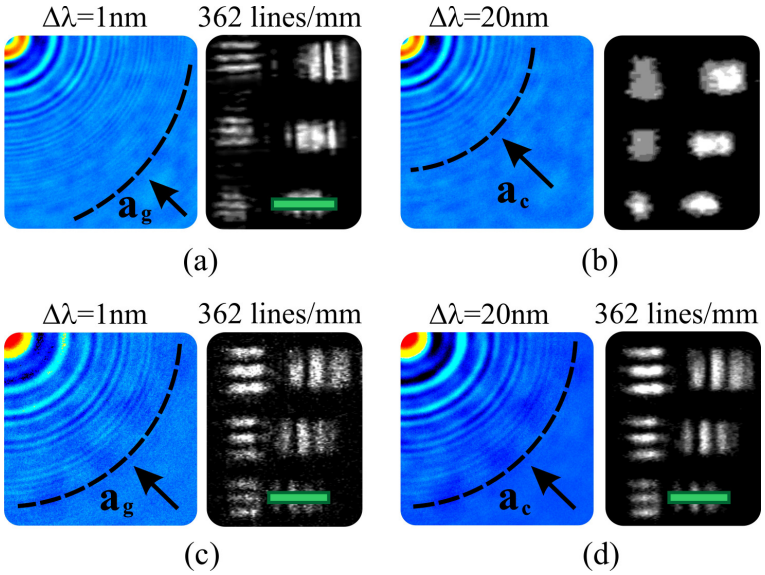

Figure 6: Image of the USAF resolution target reconstructed from monochromatic ($\Delta\lambda$ = 1 nm) and broadband ($\Delta\lambda$ = 20 nm) correlation records captured in the setup optimized for (a),(b) monochromatic and (c),(d) broadband light. The quality of the monochromatic image (c) is maintained even in the broadband image (d), provided the experimental system is optimally adjusted.

the interference fringes were strongly damped due to the partial temporal coherence of light. The interference pattern then emerged only in a significantly reduced area defined by the coherence aperture (area a_c in Fig. 6b). Reduction of the hologram aperture due to the partial temporal coherence resulted in a deterioration of the image resolution. As is evident, the image of the resolution target reconstructed with $\Delta\lambda = 20$ nm (Fig. 6b) is significantly degraded compared to the snapshot obtained for $\Delta\lambda = 1$ nm (Fig. 6a). By the theoretical nondispersive model, an optimal CCD position can be found provided the spectral bandwidth of light is specified. For $\Delta\lambda = 20$ nm, the CCD position $\Delta_2 = 1650$ mm was determined. In this setting, the optical path difference is almost zero so that the coherence aperture is extended to the same area as in the monochromatic light (area a_c in Fig. 6d). In this case, the image quality of the resolution target achieved in monochromatic light ($\Delta\lambda = 1$ nm, Fig. 6c) is preserved also in broadband light ($\Delta\lambda = 20$ nm, Fig. 6d).

4.2. Spiral and Bessel beam imaging

A significant part of the doctoral thesis is focused on the development of holographic microscopy and methods of advanced imaging based on the recent discoveries of singular and nondiffracting optics. A special attention was devoted to optical vortices and nondiffracting Bessel beams that were deployed in techniques of the correlation imaging and digital holography. The vortex phase structures and the self-imaging effects of nondiffracting beams were optimized in imaging applications and applied to the edge contrast enhancement in the spiral incoherent correlation imaging and utilized for three-dimensional localization of microscopic objects by the DH PSF.

4.2.1. Edge enhancement in spiral correlation imaging

The spiral imaging is a novel technique of microscopy utilizing interference of optical vortices for the edge contrast enhancement of weakly scattering specimens [38]. In [20], the principles of the spiral microscopy were successfully implemented in the correlation holographic imaging, working with spatially incoherent light. The method benefited from a hybrid coherence regime of the correlation imaging, in which the incoherently recorded holograms were coherently reconstructed [18]. The optical vortices utilized in the spiral correlation imaging can be implemented either optically or digitally, resulting in edge contrast enhancement of three-dimensional amplitude objects

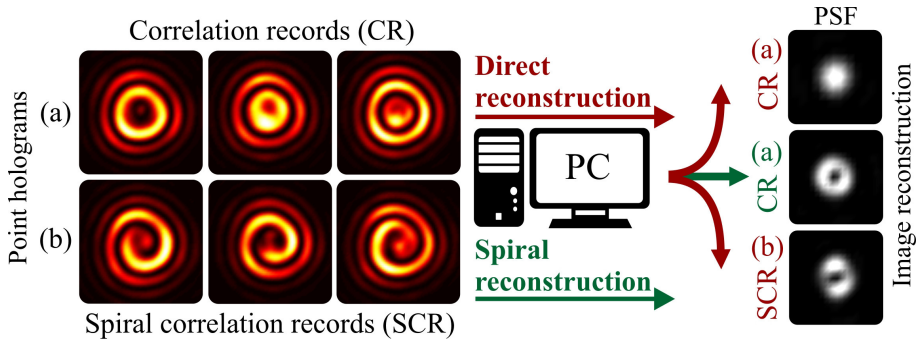

Figure 7: Illustration of optical and digital implementation of the spiral correlation imaging. The standard point correlation records CR (top row (a)) can be processed by direct or spiral reconstruction resulting in the Airy pattern (red CR (a) PSF) or the doughnut vortex spot (green CR (a) PSF). The direct reconstruction of the spiral correlation records SCR prepared with a vortex reference wave (bottom row (b)) results in the doughnut vortex image (red SCR (b) PSF).

In optical implementation of the spiral correlation imaging, the individual point holograms are created by interference of the spherical signal wave and the vortex reference wave. The waves are created by the SLM in the standard optical arrangement shown in Fig. 3. By processing the point spiral records, the vortex hologram representing a virtual diffractive lens with the helical phase is obtained [18,20]. Reconstruction of the point vortex hologram is performed by the Fresnel transform. Instead of the Airy pattern appearing in the standard correlation imaging, the vortex image is created. In the digital implementation of the spiral correlation imaging, the spatial spectrum of the standard image reconstruction is modulated by a spiral phase mask and the vortex image is obtained using records created by the interference of spherical waves.

Experimental results demonstrating the edge contrast enhancement and application potential of the spiral correlation imaging are shown in Figs. 7 and 8. In all experiments, a low aperture MO ($NA_0 = 0.15$, $f_0 = 150$ mm) and the spherical and reference waves with $f_s = 470$ mm and $f_r = 523$ mm were used. Optionally, a helical phase with the topological charge $l = 1$ was imposed on the reference wave. The CCD was fixed at the distance $\Delta_2 = 495$ mm behind the SLM. Using point correlation records, both optically and digitally implemented spiral correlation imaging is demonstrated in Fig. 7. In the left panel, the point correlation records CR are shown (row (a)), which were obtained by interference of the spherical signal and reference waves. The spiral point correlation records SCR (row (b)) were captured, when the spherical signal wave and the vortex reference wave with the topological charge $l = 1$ were used. The variability of the method is further

enhanced by a possibility to apply the direct reconstruction (red arrows) or the spiral reconstruction (green arrow) of the correlation records. When standard point records CR are directly reconstructed, the Airy pattern is obtained (right panel in Fig. 7, red CR (a) PSF). Applying the direct reconstruction algorithm to spiral SCR point records, the doughnut spiral PSF appears (right panel in Fig. 7, red SCR (b) PSF). The nearly perfect vortex images can be created by the spiral reconstruction of the standard point records CR (right panel in Fig. 7, green CR (a) PSF), providing the edge contrast enhancement digitally.

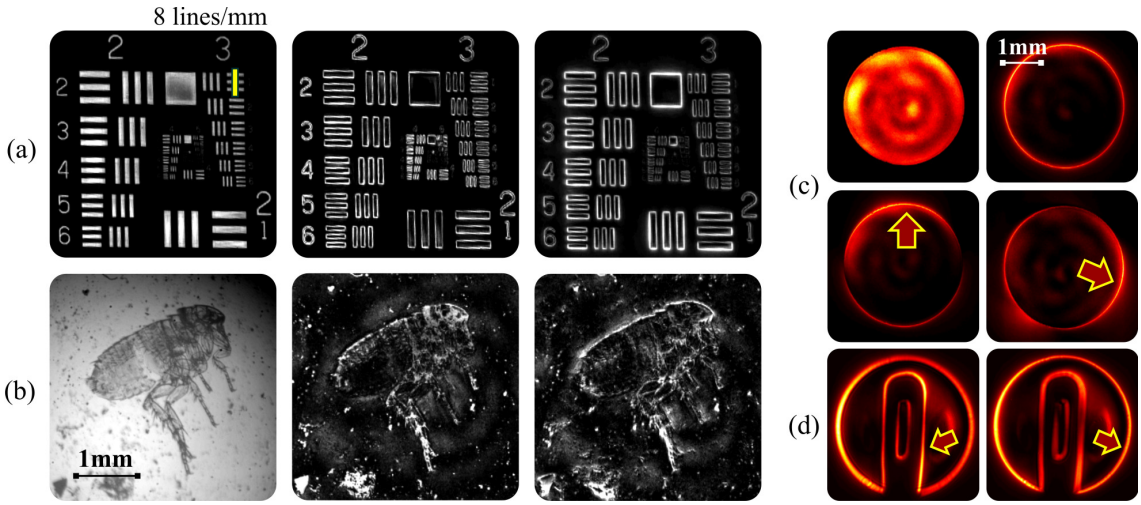

Figure 8: Snapshots demonstrating spiral correlation imaging. (a) Images of the USAF resolution target obtained by standard correlation imaging using spherical signal and reference waves (left) and optical (middle) and digital (right) spiral correlation imaging. (b) Images of the flea obtained by optical imaging (left) and standard (middle) and spiral (right) correlation imaging. (c) Images of a circular aperture obtained by standard correlation imaging and isotropic edge contrast enhancement (first row) and anisotropic edge contrast enhancement in two different directions indicated by arrows (second row). (d) Edge contrast enhancement in three-dimensional spiral imaging demonstrated by a needle placed in front of the circular aperture (left-needle in focus, right-aperture in focus).

Practical applicability of spiral correlation imaging is assessed in Figs. 8a,b, where the results of the spiral correlation imaging are compared to the standard images. In the top row, the images of the USAF resolution target are shown, which were obtained by standard correlation imaging (left) and optically (middle) and digitally (right) implemented spiral imaging. In the bottom row, the direct optical image of a flea (left) is compared to the standard correlation image (middle) and the spiral image exhibiting edge contrast enhancement (right). Modifying basic experiments of spiral microscopy [38], the anisotropic and three-dimensional edge contrast enhancement were also demonstrated. The experimental results obtained are presented in Figs. 8c,d, where a blank circular aperture and needle were used as a test object. The snapshots in the top row of Fig. 8c demonstrate the standard reconstruction of the aperture and its spiral reconstruction with the isotropic edge contrast enhancement. The snapshots in bottom row of Fig. 8c show spiral reconstruction of the aperture with anisotropic edge enhancement performed in two different directions (preferred directions indicated by arrows). A successful combination of the correlation holography with the spiral imaging allowed the first demonstration of the edge

contrast enhancement in three-dimensional imaging [20]. Results of the experiment are shown in the Fig. 8d. As a simple three-dimensional object, a needle placed in front of a circular aperture was used. The snapshots demonstrate edge contrast enhancement in the images, where the needle and the aperture are in focus. The refocusing indicated by arrows was achieved by processing the same correlations records.

4.2.2. Axial localization by rotating Bessel beams

The methods of axial localization and tracking of particles were thoroughly studied in the last decade and several techniques providing a full volume information about observed samples were proposed. In most localization experiments, the DH PSF has been used. Its intensity spot is composed of two bright lobes, whose angular position is changed during defocusing. Recently, various modifications of the basic experiment of the rotating imaging [39,40] emerged, employing both radial and azimuthal sampling of a spiral phase mask [41–43]. The axial localization by the DH PSF has become a significant technique, which allowed the superresolution imaging in three-dimensional fluorescence microscopy [44]. In the doctoral thesis, the original methods of axial localization were developed, in which the DH PSF was implemented in digital holography and optical microscopy. In both methods, the DH PSF was realized by nondiffracting Bessel beams.

Rotating vortex imaging in digital holography

In digital holography, the DH PSF can be implemented by purely digital tools without technical modification of the conventional experiments, working with both spatially coherent and incoherent light. The digital implementation of the rotating DH PSF is obvious from Fig. 9 illustrating virtual optical system used in the post-processing of standard holographic images [19,45]. The complex amplitude of the image obtained by the hologram reconstruction u' is further processed by the Fourier transform. In optical analogy shown in Fig. 9, the holographic image is placed near the front focal plane of the virtual Fourier lens L_1. Behind the Fourier transforming lens, the digital spiral filter is applied to the spatial spectrum of the holographic image. Two different types of digital filters S_N and S_I were designed, resulting in generation of a single nondiffracting vortex beam and a vortex self-imaging, respectively. After performing inverse Fourier transform by the virtual lens L_2, the complex amplitude of the image is obtained as

$$u'_R = \mathrm{iFT}\{S_j \cdot \mathrm{FT}(u')\}, \quad j = N, I. \tag{2}$$

Further processing of the complex amplitude is different for both types of filters and will be discussed separately.

Rotating imaging with single nondiffracting vortex beam

Rotating imaging with single nondiffracting vortex beam is implemented by the spiral phase modulation performed by a thin annular digital filter placed at the intermediate plane of the virtual 4-f system (Fig. 9a). In simplifying calculations demonstrating principle of the method, the transparency of the spiral filter can be written by the Dirac delta function

$$S_N = \delta(F - F_0)\exp(il\varphi), \tag{3}$$

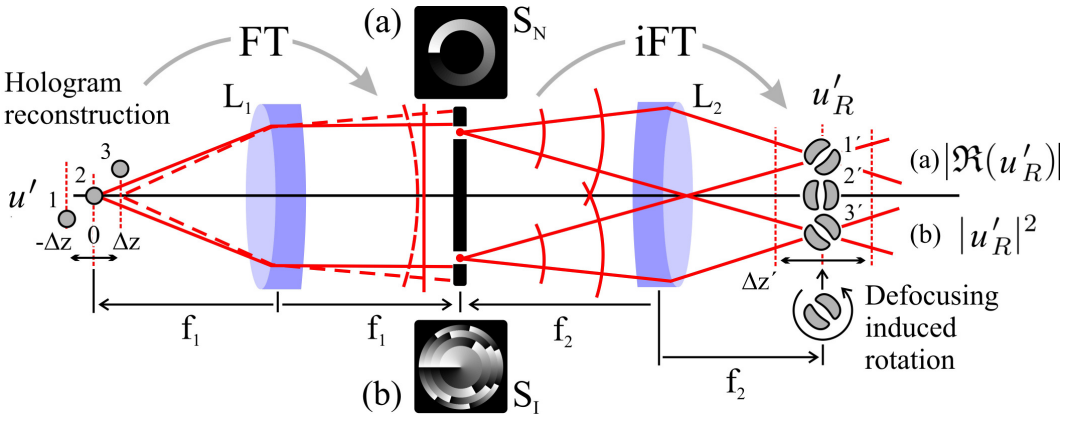

Figure 9: Implementation of the rotating DH PSF in methods of digital holography and correlation imaging. Spatial spectrum of the reconstructed image is digitally modulated in a virtual 4-f system composed of lenses L_1 and L_2. By the spiral phase modulation, single non-diffracting vortex beam (a) or superposition of nondiffracting vortex modes (b) are created, providing the asymmetrical rotating point images either in real part of the complex amplitude $|\Re\{u'_R\}|$ or the image intensity $|u'_R|^2$.

where (F, φ) are the cylindrical coordinates at the Fourier plane, F_0 is the radius of the thin annular filter and l denotes the topological charge of the spiral phase modulation. Substituting (3) into (2) and using u' related to the axial object point, the complex amplitude of the rotating image is obtained. The asymmetry required for a depth estimation from the image rotation is not available in the intensity but in the real part of the complex amplitude u'_R. In order to work with positive values, the absolute value of the real part is used,

$$\left|\Re(u'_R)\right| \propto \left|J_l \cos(l\varphi' + \Phi)\right|. \tag{4}$$

The image spot (4) is obtained by multiplying the symmetrical Bessel function of the first kind and l-th order by the cosine function depending on the defocusing Δz_0 through the term $\Phi \equiv \Phi(\Delta z_0)$. As a result, the doughnut profile determined by the Bessel function with the azimuthal cosine modulation is obtained. In the azimuthal direction, $2l$ bright maxima appear, whose angular position changes due to the object space defocusing Δz_0. A continuous change of position of the point object thus leads to the rotation of its image. By evaluating the angular rotation of the image, the position of the corresponding point object is determined with the high accuracy. In experiments, the topological charge $l = 1$ is most widely used providing a two-lobe image corresponding to the DH PSF.

Accuracy and applicability of the method were assessed in configuration for incoherent correlation imaging. During the hologram acquisition the MO Melles Griot ($NA_0 = 0.55$, $f_0 = 4$ mm) and the recording configuration with plane reference and spherical signal waves ($f_r \to \infty$, $f_s = 400$ mm) was utilized, while the CCD was placed at the position $\Delta_2 = 600$ mm. The DH PSF was created digitally using the spiral phase filter with $l = 1$. The accuracy was evaluated using a standard deviation of the measured rotation angle $\overline{\Delta\varphi}$. By processing the measured data, the standard deviation $\overline{\Delta\varphi} = 1.27°$ was obtained. For the used numerical aperture $NA_0 = 0.25$ and the determined standard deviation of angle evaluation $\overline{\Delta\varphi}$, the accuracy of the axial localization 1 μm was estimated. The applicability of the method was evaluated using, the fluorescent and polystyrene beads as the point objects to be localized. In the fluorescence experiment, the fixed fluorescent

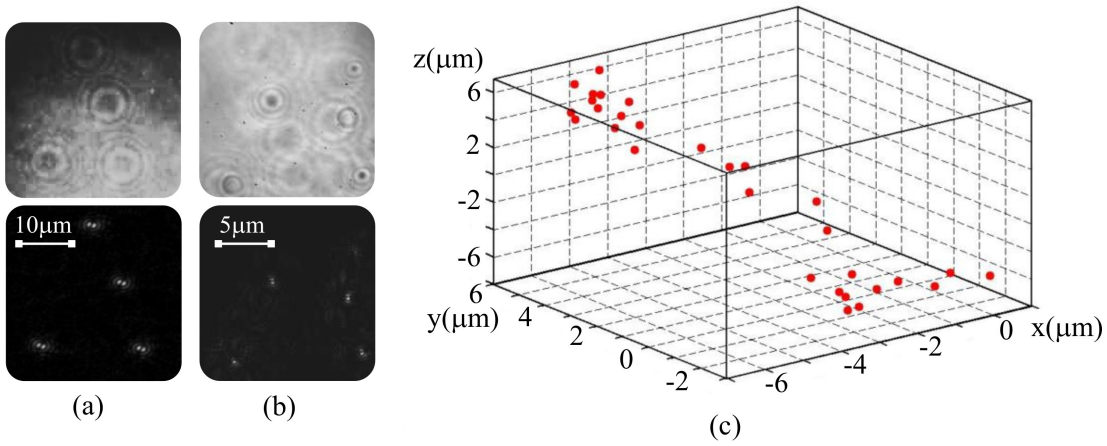

Figure 10: Three-dimensional localization and tracking of microscopic particles based on the rotation of a single nondiffracting vortex beam. (a) Hologram of fixed 5 μm fluorescent beads (top) and its reconstruction providing the DH PSFs of the individual beads (bottom). (b) The same as in (a) but for 0.5 μm polystyrene beads moving by Brownian motion. (c) Three-dimensional trajectory of a selected polystyrene bead. Individual positions were reconstructed from holograms recorded with the frame frequency 10 Hz.

beads (Invitrogen, diameter 5 μm) were defocused by a precisely controlled displacement and the expected image rotation was examined. In the advanced experiments, the axial localization and particle tracking were tested. The polystyrene beads (diameter 0.5 μm) moving by the Brownian motion were used as a sample and the holograms recorded on the CCD. The holograms and their reconstructions providing the DH PSFs for individual beads are shown in Figs. 10a,b. In the experiment with the polystyrene beads, the rotation of the DH PSF was utilized for a precise axial localization and tracking of a selected particle. As the result, the trajectory of the selected polystyrene bead was created, with the accuracy in unites of micrometers in all three dimensions (Fig. 10c). Individual holograms contributing to the particle tracking experiment were captured with the frame frequency 10 Hz.

Self-imaging of nondiffracting vortices in digital holography

Axial localization of the particles can also be accomplished by intensity processing of the reconstructed vortex image. In this case, two or more nondiffracting vortex beams are required, whose interference creates asymmetrical image rotating under defocusing. A cooperation of the nondiffracting vortex beams resulting into the effect known as self-imaging can be extremely advantageous for the localization experiments. In order to achieve the self-imaging, the special spiral mask is used in a virtual 4-f system during post-processing of the standardly reconstructed image (Fig. 9b). The transparency of the spiral mask can be written as

$$S_I(F,\varphi) = \begin{cases} \sum_{n=1}^{N} \exp(il_n\varphi), \text{ for } R\sqrt{\frac{n-1}{N}} < F < R\sqrt{\frac{n}{N}},\ n = 1,2,...N, \\ 0, \text{ for } F > R, \end{cases} \tag{5}$$

where (F,φ) are the cylindrical coordinates at the focal plane of the lens L_1 and R is the maximal radius of the mask. The radius of the mask is divided into N radial zones, where the spiral phase modulation with the topological charge l_n assigned to the n-th zone is

introduced. Substituting (5) into (2), the complex amplitude of the rotating image u'_R is obtained. By calculating the image intensity $I'_R = |u'_R|^2$, the rotating PSF is obtained,

$$I'_R = \sum_{n=1}^{N} J_{l_n}^2 + 2 \sum_{n=1, n<n'}^{N} \sum_{n'=n+1}^{N} J_{l_n} J_{l_{n'}} \cos(\Omega_{n,n'}), \tag{6}$$

where

$$\Omega_{n,n'} = [(l_n - l'_n)\varphi' + (\Phi_n - \Phi'_n)]. \tag{7}$$

The total intensity I'_R is composed of the annular intensity spots of the individual vortex beams given by $J_{l_n}^2$ and the interference terms depending on the phase factors $\Omega_{n,n'}$. The symmetrical annular spots are azimuthally modulated by the cosine functions creating bright maxima. Since the cosine arguments depend on Δz_0 through Φ_n, the bright maxima rotate along the rings, if defocusing occurs in the object space. The rigid rotation of the image is inherently achieved provided the parameters of the nondiffracting vortex beams satisfy the self-imaging condition and the topological charge of the n-th vortex mode is given by $l_n = l_0 + n\Delta l$, where l_0 is an arbitrary integer and $\Delta l = l_{n+1} - l_n$ denotes the difference of the topological charges between two neighboring modes.

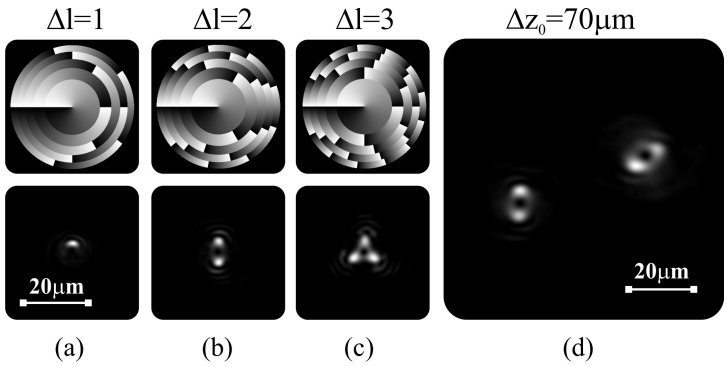

Figure 11: Experimental demonstration of the axial localization in the incoherent correlation imaging with the rotating PSF obtained by the self-imaging of nondiffracting vortex modes. Spiral mask (top) and reconstructed PSF (bottom) for the superposition of $N = 5$ vortex modes and the difference of the topological charges (a) $\Delta l = 1$, (b) $\Delta l = 2$ and (c) $\Delta l = 3$. (d) Determination of the mutual axial distance of two point sources ($\Delta z_0 = 70$ μm) from the relative angular rotation of the DH PSFs.

The proposed method was assessed experimentally in the system for incoherent correlation imaging. Experiments were performed in the setup using the MO Melles Griot ($NA_0 = 0.28$, $f_0 = 20$ mm), plane reference and spherical signal waves ($f_r \to \infty$, $f_s = 750$ mm) and a CCD at the position $\Delta_2 = 950$ mm. The point-like source was substituted by a single mode optical fiber, while the rotating PSFs were created by the spiral masks with the parameters $N = 5$, $l_0 = 0, -1, -2$ and $\Delta l = 1, 2, 3$, respectively. Obtained single-lobe corkscrew PSF, DH SPF and the rotating PSF with three bright lobes are presented in Fig. 11. In the localization experiment with DH PSF, two point-like sources were separated both laterally and axially and their holograms recorded. Determining the relative angular rotation of the DH PSFs, the axial separation distance of the point-like sources $\Delta z_0 = 70$ μm was found (Fig. 11d).

Self-imaging of nondiffracting vortices in optical microscopy

In the doctoral thesis, the radial sampling of the spiral phase mask was applied and new technique of the axial localization proposed, in which a self-imaging of nondiffracting vortices was utilized [45]. Although the original idea was presented as an extension of the holographic imaging, the principle of the method was also successfully applied to optical microscopy. As the main advantages of these methods, a significantly extended working range, resistance against aberrations and dark-filed effect were demonstrated [17].

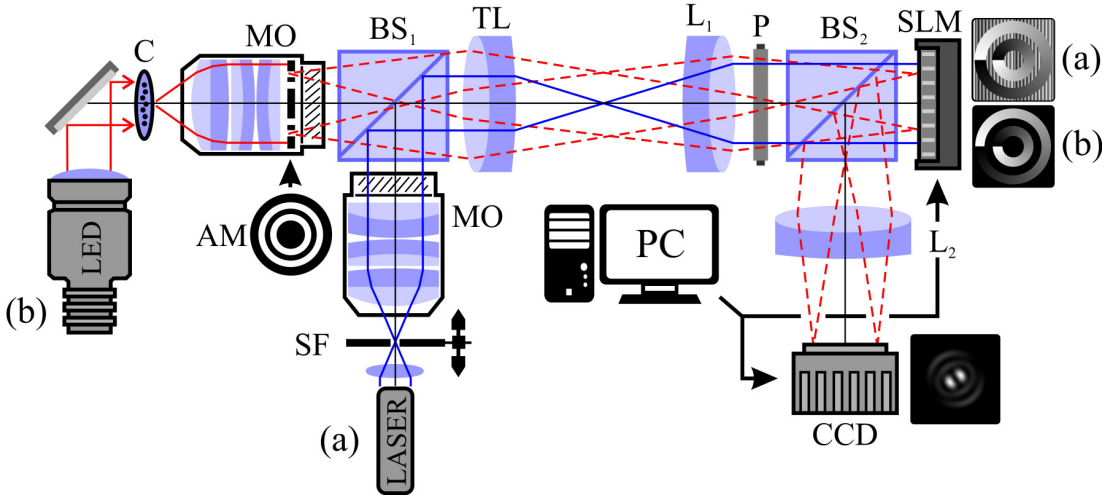

Figure 12: All-optical arrangement for the axial localization by vortex self-imaging. (a) Optical path for system adjustment and testing using point source created by a spatial filter SF. (b) Optical path for advanced experiments with polystyrene and fluorescent beads suspended in a glass capillary C. Abbreviations used: MO-microscope objective, AM-amplitude filter, $BS_{1,2}$-beam splitter, P-polarizer, TL-tube lens, $L_{1,2}$-Fourier lenses.

The self-imaging of nondiffracting vortex modes was tested experimentally in the setup shown in Fig. 12. The all-optical system is based on bright-field microscope supplemented by a modular part. The image is formed due to the same spiral modulation that was used in the digital holography to achieve the self-imaging [45]. Contrary to the previous demonstrations [45], only two modes generated from the mask zones with a varying width were used in the experimental testing. The required complex modulation, including both amplitude and phase modulation, was introduced by two different techniques shown in Figs. 12a,b. In the first approach (Fig. 12a), the phase-only SLM was used. Since in addition to the spiral phase modulation also the amplitude modulation was necessary, the special CGHs were prepared and displayed on the SLM. Instead of the amplitude attenuation of incident light, a blazed grating was applied in the desired areas of the mask, deflecting light away from the optical path used. In an alternative approach (Fig. 12b), the complex modulation was introduced in two steps. Using a custom fabricated amplitude filter, the bright nondiffracting modes with $l = 0$ were created at the back focal plane of the MO. Subsequently, the vortex phase was assigned to individual nondiffracting modes by the SLM placed at the plane optically conjugated with the MO pupil.

Extension of the working range and the aberration robustness were tested in the setup shown in Fig. 12a. As a point source, the spatially filtered He-Ne laser was used. Light from the spatial filter SF was collimated by the MO Newport ($NA_0 = 0.4$, $f_0 = 9$ mm)

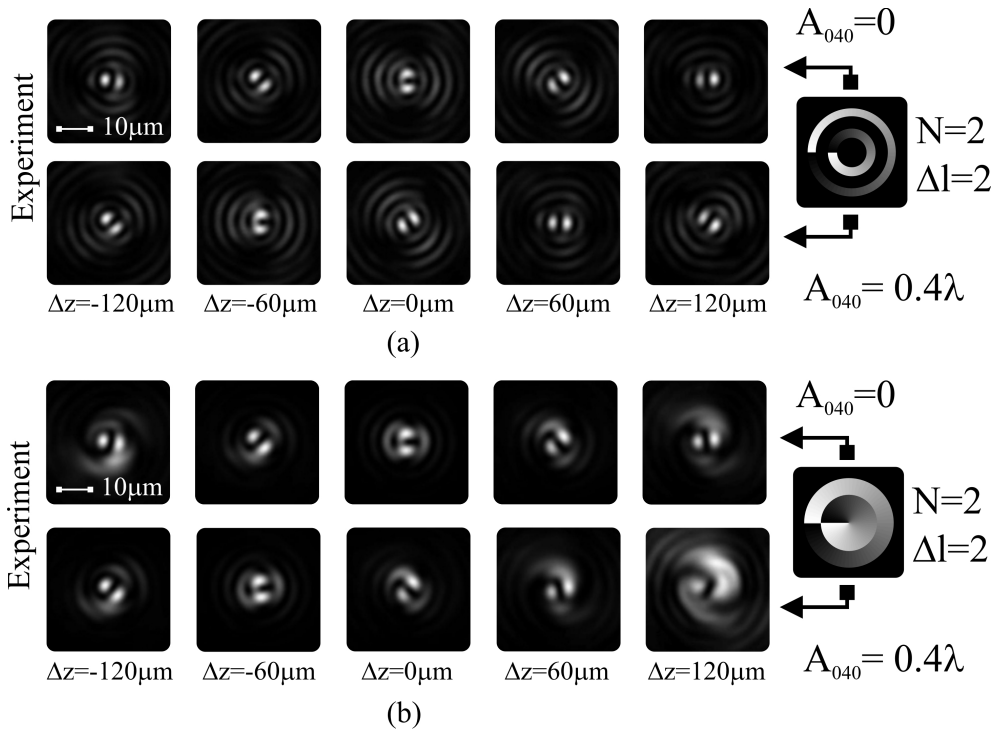

Figure 13: Experimental results on all-optical axial localization using two-mode vortex self-imaging. (a) Aberration resistant rotation of the DH PSF realized by the spiral mask with thin annular zones (top row - without aberration, bottom row - spherical aberration $A_{040} = 0.4\lambda$). (b) Aberration deterioration of the DH PSF realized by the spiral mask with two wide zones (top row - without aberration, bottom row - spherical aberration $A_{040} = 0.4\lambda$). In both demonstrations, the object space axial range $\Delta z = \pm 120$ μm and the mask parameters $N = 2$ and $\Delta l = 2$ were used [17].

and by the beam splitter BS_1 diverted towards the tube lens TL ($f_T = 200$ mm) and the 4-f system composed of the lenses L_1 and L_2 ($f_1 = 200$ mm, $f_2 = 400$ mm). The phase-only SLM was placed at the back focal plane of the lens L_1. The spiral mask addressed on the SLM was composed of two thin annular zones with the radii $R_1 = 0.64$ mm and $R_2 = 0.9$ mm, which were modulated by the vortex phase with $l_1 = -1$ and $l_2 = 1$ ($l_0 = -3$, $\Delta l = 2$). To demonstrate the aberration robustness of the axial localization, the third-order spherical aberration $A_{040} = 0.4\lambda$ was added on a defocused wavefront. The aberration was created by the SLM together with the spiral mask, in order to achieve a full control over the wavefront deformation. Results obtained with the thin annular zones ($\Delta R = 0.1$ mm) are presented in Fig. 13a. The rotating DH PSF acquired in the system with well corrected spherical aberration ($A_{040} = 0$) is compared with the case, in which the spherical aberration $A_{040} = 0.4\lambda$ was added by the SLM. In both experiments, the rotation of the DH PSF was monitored within the axial range $\Delta z = \pm 120$ μm. As is apparent, the shape of the DH PSF is not affected by aberrations and only some additional angular rotation can be observed. Since the rotation remains the same for all depths, aberration effects can be effectively compensated [17]. In Fig. 13b, the annular zones were extended and fully transmitting areas created. When the mask with two fully transmitting zones was used, the self-imaging condition was disrupted and an apparent deformation of the image spot occurred for larger defocusing. It is evident from comparison of the top rows of Figs. 13a and 13b, where the same axial localization range $\Delta z = \pm 120$ μm was used.

As shown in the bottom row of Fig. 13b, the resistance against aberrations was lost in experiment performed with fully transmitting zones of the mask.

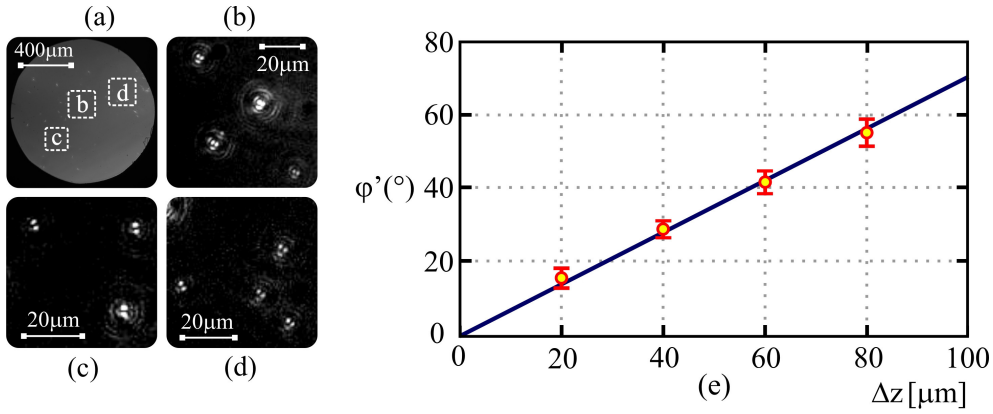

Figure 14: Axial localization of polystyrene beads by the rotating DH PSF using two-mode vortex self-imaging. (a) Polystyrene beads (diameter 1 μm) suspended in a glass capillary tube. (b-d) Angularly rotated images of polystyrene beads in magnified portions of the entire field of view shown in (a). (d) Evaluation of the localization accuracy in the presence of spherical aberration randomly selected from the interval $A_{040} =\in \langle -0.4\lambda, 0.4\lambda \rangle$. The standard deviation at individual positions was determined by processing 40 records made using the spiral mask with two thin annular zones ($N = 2$, $\Delta R = 0.1$ mm) and the topological charges $l_1 = -1$ and $l_2 = 1$ ($l_0 = -3$, $\Delta l = 2$).

A possibility to eliminate the additional image rotation caused by aberrations was further examined using the mask with thin annular zones. In the localization experiments, the spherical aberration randomly selected from the interval $A_{040} \in \langle -0.4\lambda, 0.4\lambda \rangle$ was imposed on the defocused wavefront. Subsequently, the dependence of the rotation angle on the object space defocusing was measured. By processing experimental data, the additional rotations caused by the spherical aberration were eliminated and experimental dependence of the rotation angle on the defocusing compared with a theoretical linear dependence (Fig. 14e). The standard deviations in measured positions were obtained by processing 40 records.

The practical applicability of the method was tested in the experimental configuration shown in Fig. 12b. As the sample, a glass capillary tube with suspended polystyrene beads (diameter 1 μm) was used. The polystyrene beads moved freely by the Brownian motion. Due to high pass filtering accompanying the spiral filtration, dark-field effect was achieved and the rotating images with good contrast were successively recorded on the CCD with a frame frequency 5 Hz. The entire field of view and its magnified portions with the rotating images are shown in Figs. 14a-d.

5. Outcomes of applied research

In the doctoral thesis, the original imaging concepts of the correlation and holographic microscopy were developed. In experiments carried out, technical drawbacks were revealed, that have become a challenge for the further elaboration and enhancement of the techniques being developed. The main achievements can be summarized as follows:

- In the incoherent correlation imaging shown in Fig. 3, a full overlapping of the signal and reference waves was achieved only for recording of the axial object point and the interference disappeared even at a very small field of view. This problem was successfully solved in the setup supported by relay optics [12]. In the modified system, the accessible field of view was significantly enhanced and the optimal resolution retained in the entire recorded area.

- Extremely strong diffractive dispersion preventing utilization of the SLM in broadband imaging was effectively eliminated by an afocal refractive corrector, which was designed, manufactured in Meopta-optika, s.r.o. and tested in the laboratory [13].

- Exploiting the birefringence of liquid crystal molecules, new method of a motionless phase-shifting was proposed and implemented in the polarization adapted Mirau interferometer [15].

- As the main application output benefiting from partial results of the doctoral thesis, a multimodal microscope aided by the SLM technology was designed and realized in the IPE BUT laboratory. The prototype of the microscope has become one of the significant results of the project CDO supported by the TA CR.

5.1. Incoherent correlation imaging with extended field of view

In optical microscopy, the field of view is clearly defined by parameters of the MO or field diaphragms, respectively. The situation is more complicated in the incoherent correlation imaging, where the image is not detected directly but reconstructed from point correlation records created by interference of the signal and reference waves. Required interference occurs provided a spatial overlapping of the signal and reference waves at the CCD is achieved. In the previously used setups, the signal and reference waves obtained by splitting light from off-axis points were spatially separated at the CCD and interference was impossible even in a small portion of the field of view of the MO (Fig. 15a).

Loss of interference due to the insufficient spatial overlapping of the signal and reference waves was successfully solved by applying a relay optical system inserted between the MO and the SLM [12]. In the modified setup, the relay lens L_1 and L_2 form a 4-f system adjusted such that the exit pupil of the MO is optically conjugate with the SLM plane. As the ray paths in Fig. 15b show, the input beam is precisely centered on the SLM and the signal and reference beams perfectly overlap on the CCD for all off-axis points of the object.

The proposed configuration [12] was assessed experimentally using the MO Melles Griot ($NA = 0.28$, $f_0 = 20$ mm), the spherical signal and plane reference waves ($f_s = 247.5$ mm, $f_r \to \infty$) and the separation distance $\Delta_2 = 495$ mm. In experiments without relay lenses, the minimal achievable distance between the MO and the SLM $\Delta_1 = 270$ mm was set. In improved experiments, the 4-f system with two identical relay lenses L_1 and

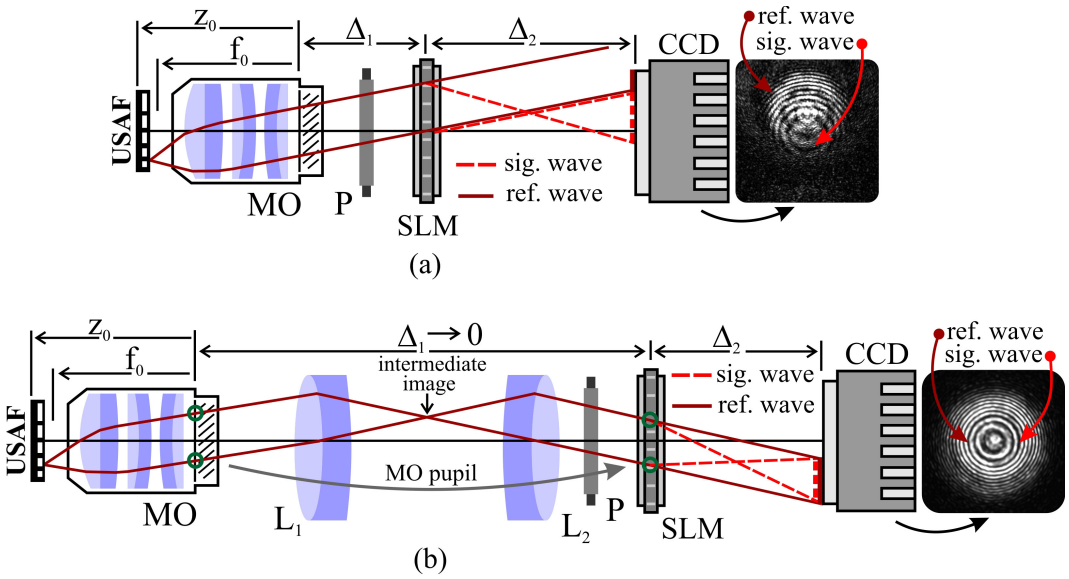

Figure 15: Optical arrangements of the incoherent correlation imaging. (a) Original configuration [28] with decreasing overlapping of interfering waves for off-axis points and the strongly reduced accessible field of view. (b) Improved configuration supplemented by the relay optics [12] and providing the perfect overlapping of interfering waves in the entire field of view of the MO.

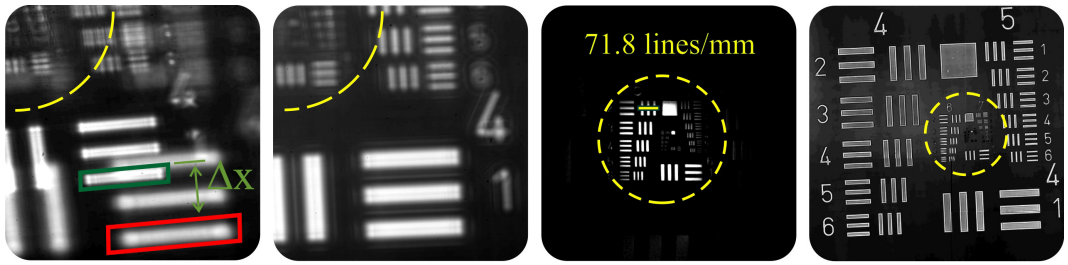

Figure 16: The correlation records and the image reconstructions of the USAF resolution target realized in the original setup of the incoherent correlation imaging [28] (a),(c) and the improved system with the relay lenses [12] (b),(d). (a) Corrupted correlation record (system in Fig. 15a) with unacceptable separation Δx of signal wave (green box) and reference wave (red box) in peripheral part of the field of view (sufficient overlapping indicated by yellow dashed line). (b) Perfect overlapping of interfering waves in the entire field of view of the MO (system in Fig. 15b). (c) Strongly reduced field of view in the image obtained by the digital reconstruction of the record (a). (d) Full field of view in the image obtained by the digital reconstruction of the record (c). In the reconstructed images (c) and (d), the same areas of the field of view are indicated by the yellow circles.

L_2 ($f = 150$ mm) was applied. In both systems, the holographic records and the image reconstructions were performed to demonstrate progress achieved with the relay optics. Experimental results obtained with the USAF resolution target are shown in Fig. 16. In the records carried out in the original system Fig. 15a, the significant lateral shift between the signal and reference beams was observed (Δx in Fig. 16a). In accordance with theory, the separation distance Δx was increased in the peripheral part of the field of view and sufficient overlapping was achieved only in the circular area denoted by the yellow dashed

line. The records of the USAF resolution target shown in Fig. 16b were acquired with the relay lenses so that the perfect correlation overlapping of signal and reference beams was obtained in the entire field of view of the MO. The deteriorated and perfect holographic records of the USAF resolution target (Figs. 16a,b) were processed numerically and the images were reconstructed. In the setup without relay optics, the image reconstruction was successful in only a small part of the field of view denoted by the yellow dashed line in Figs. 16a,c. The image reconstruction in a significantly enlarged field of view (Fig. 16d) was reached with the record taken using the relay optics (Fig. 16b).

5.2. Correction of diffractive dispersion in broadband SLM imaging

The SLM is a versatile light shaping device with a multitude of optical applications. However, specific operating conditions have to be respected for an optimal modulation of light. If the broadband light is used, the operation of the SLM is impaired by the effects caused by both refractive and diffractive dispersion. In the doctoral thesis, the attention has been focused on the diffractive dispersion accompanying the quadratic phase modulation. The proposed correction technique is important for lens-like SLM applications, including light focusing in both the incoherent correlation imaging and the standard optical imaging with a direct image detection [13].

Principle of the proposed achromatic correction of the SLM using an afocal refractive system is schematically illustrated in Fig. 17. The corrector was designed as afocal so the performance of the SLM lens was not impaired for the central wavelength λ_0. For other wavelengths of the spectrum, a non-zero optical power of the corrector was introduced (Fig. 17a) resulting in the refractive chromatic aberration just compensating effects of the diffractive dispersion of the SLM lens. Due to a contradictory effect of the refractive and diffractive dispersion, their mutual compensation is possible, provided the condition of the achromatic imaging is satisfied [13],

$$\frac{1}{V_1} - \frac{1}{V_2} + \frac{1}{\kappa V_D} = 0, \tag{8}$$

where V_1 and V_2 are the Abbe numbers of the front and rear corrector lenses, V_D is the Abbe number of the SLM lens and κ is the ratio of the focal lengths of the SLM lens and the front corrector lens. Prototype of the achromatic corrector was custom fabricated in the company Meopta-optika, s.r.o.

The afocal corrector was tested experimentally in conjunction with the SLM used as a tube lens in bright-field microscope. Broadband light with the spectral bandwidth $\Delta\lambda = 80$ nm was used to examine the achromatic imaging provided by the system composed of the corrector and the SLM lens (Fig. 18). In order to demonstrate the benefits of the corrector, imaging by the uncorrected SLM lens impaired by a strong diffractive dispersions was also examined. In measurements, the lenses with the numerical aperture $NA = 0.02$ and $NA = 0.06$ were gradually addressed on the SLM. In ray optics measurements, the achromatic correction was verified to be in a good agreement with the theory. The measured secondary spectrum was approximately eight times smaller than the chromatic focal shift of the uncorrected SLM lens [13]. Subsequently, the Modulation Transfer Function (MTF) was measured for both corrected and uncorrected SLM lens. Results of the measurement are demonstrated in Fig. 18a,b and compared with the theoretical MTF

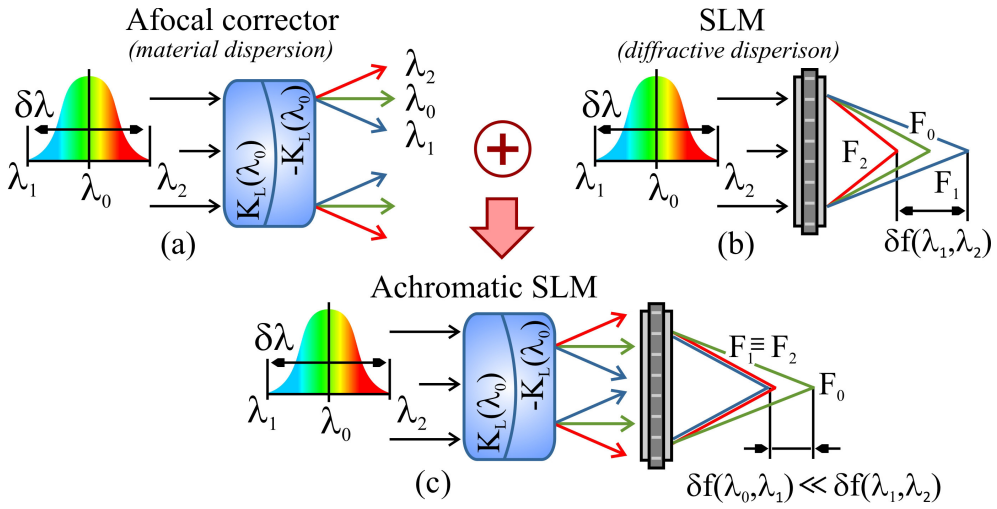

Figure 17: Concept of the dispersion compensation of the SLM: (a) material dispersion of the afocal refractive corrector, (b) diffractive dispersion of the SLM and (c) achromatic correction of the SLM [13].

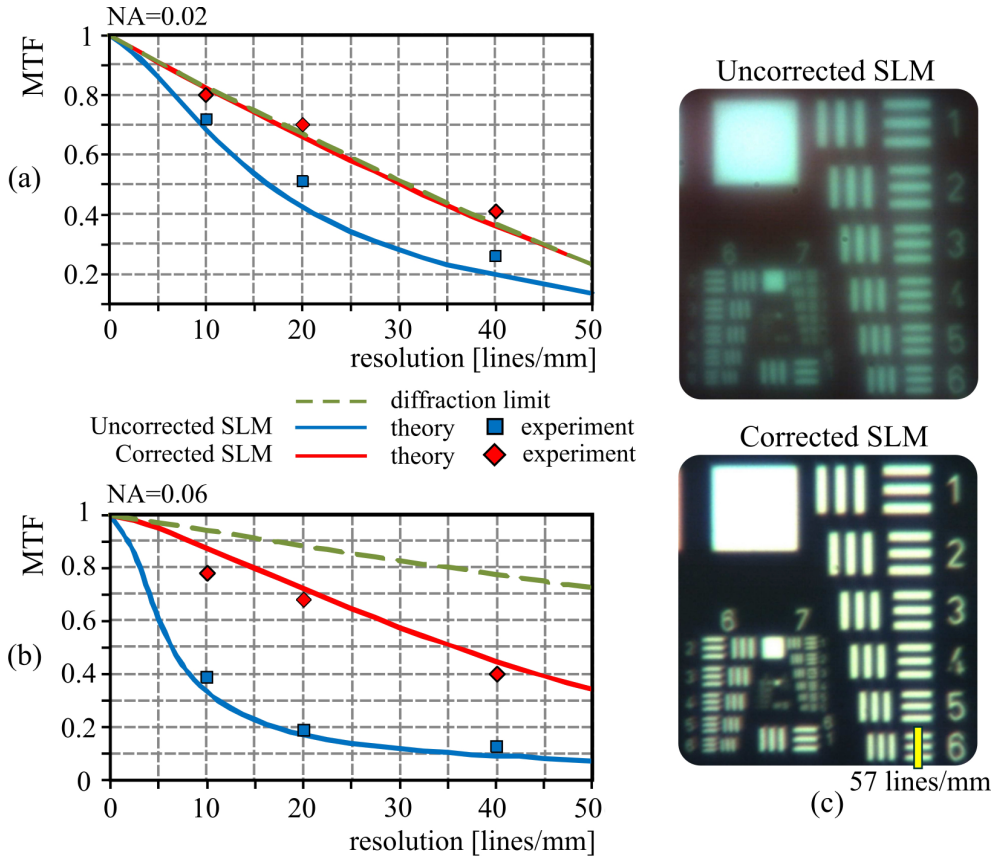

Figure 18: Experimental results demonstrating refractive afocal system for achromatic correction of the diffractive SLM lens. Comparison of the calculated and measured MTF (10, 20 and 40 cycles/mm) for the corrected and uncorrected SLM lens with the numerical aperture (a) $NA = 0.02$ and (b) $NA = 0.06$. (c) Snapshots of the USAF resolution target taken in the broadband light ($\lambda_0 = 532$nm, $\Delta\lambda = 80$ nm): uncorrected SLM lens (top), corrected SLM lens (bottom).

calculated by means of the Oslo Premium software. For the low aperture SLM lens with $NA = 0.02$ (Fig. 18a), the diffraction-limited MTF (green dashed line) nearly coincides with the theoretical curve calculated for the achromatic correction (red line). A significant decrease in the MTF calculated for the uncorrected SLM lens is demonstrated by the blue curve. Experimental data obtained for the corrected and uncorrected SLM lens are demonstrated by the red rhombs and blue squares, respectively, and fit well with the related theoretical curves. For numerical aperture $NA = 0.06$ of the SLM lens, the MTF improvement achieved with the corrector is even more pronounced and for the medium spatial frequencies contrast enhancement from 0.2 to 0.7 is reached (Fig. 18b). The significant enhancement of the optical performance achieved by the achromatic correction of the SLM is clearly demonstrated by the snapshots in Fig. 18c, taken without and with the refractive corrector.

5.3. Polarization adapted Mirau interferometry with liquid crystal variable retarder

In the doctoral thesis, a new phase-shifting technique was proposed, suitable for common-path systems working with unaffected reference wave. The method utilizes a polarization adapted Mirau Interference Objective (MIO) and enables a motionless all-optical phase-shifting [15]. The phase-shifting is based on a liquid crystal light modulation and imposed on the reference wave by the LCVR. During the experiment, linearly polarized illumination beam is divided into the reference and signal wave, having orthogonal linear polarizations at the output of the MIO. The LCVR is operated as a polarization sensitive device, working with a birefringence of liquid crystals molecules and introducing phase retardance between the output waves.

The polarization adapted Mirau interferometer working with the motionless all-optical phase-shifting is shown in Fig. 19. In the illumination part, a rotating diffuser RD is placed into the laser beam to reduce the spatial coherence. A static diffuser SD and a polarizer P support the Köhler illumination of the sample by linearly polarized light. The illumination beam is deflected by a beam splitter BS towards the MIO. The MIO is supplemented by a pair of quarter-wave plates, QWP1 and QWP2, placed into the optical paths of the reference and signal waves, respectively. The fast axis of the QWP1 coincides with the polarization direction of the input beam, while the fast axis of the QWP2 is rotated by 45°. After a double passage of the reference wave through the QWP1, the polarization direction is retained. Since the polarization direction of the signal wave is rotated by 90°, after the double passage through the QWP1 and QWP2 and the reflection from the sample, the waves with orthogonal linear polarizations are obtained at the output of the MIO. The orthogonally polarized signal and reference waves then pass through the polarization selective LCVR, where phase retardation is introduced between orthogonal polarizations by anisotropic nematic liquid crystal molecules. By the analyzer A, the orthogonal linear polarizations are projected into the same direction. It enables interference of the signal and reference waves.

Experimental testing of the polarization adapted MIO was performed in two steps, which were devoted to the phase-shifting reproducibility and accuracy of the phase recovery. During the measurement, the standard MIO (Nikon $10\times/NA = 0.3$) was used and supplemented by the QWP1 providing the required polarization modification. The QWP2 ensuring compensation of optical paths was not mounted to avoid adjustments

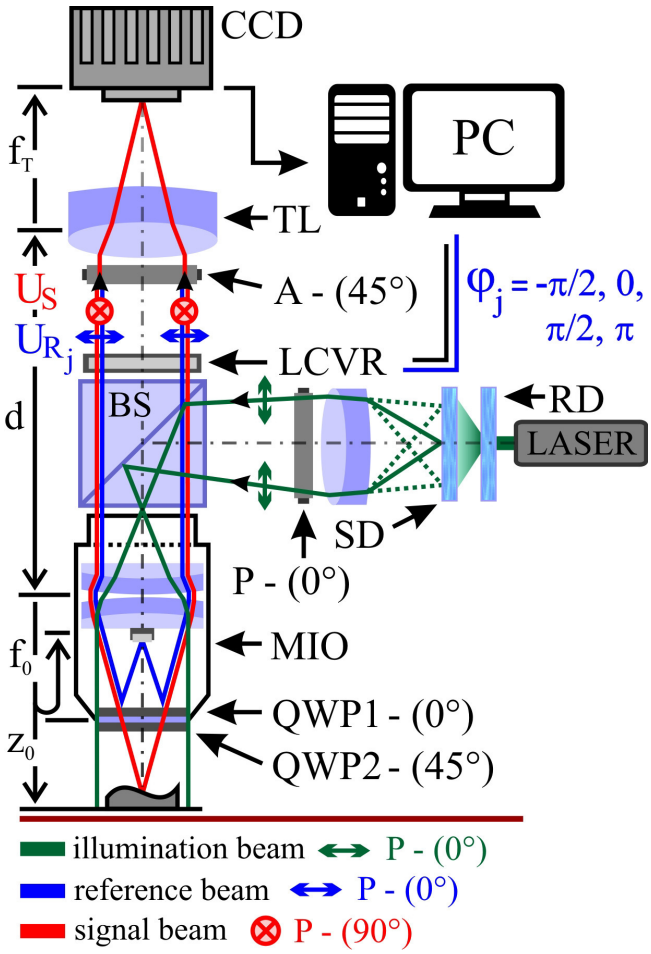

Figure 19: Polarization sensitive phase-shifting Mirau interferometer [15]: RD-rotating diffuser; SD-static diffuser; P-linear polarizer; MIO-Mirau interference objective; QWP1 and QWP2-quarter-wave plates; BS-beam splitter; LCVR-liquid crystal variable retarder; A-analyzer; TL-tube lens; CCD-charge coupled device.

inside the MIO. For testing of both phase-shifting reproducibility and phase accuracy, a tilted plane mirror introducing a linear phase retardance was used as a sample. To obtain statistical data, the measurement was repeated 99 times. From the phase reconstruction carried out in the individual measurements, an average phase $\Delta\Phi_A$ was calculated and used to evaluate the standard deviation σ_A over all realizations. The standard deviation σ_A evaluated by the average phase $\Delta\Phi_A$ gives information about the reproducibility of the phase shifts provided by the LCVR. Examining the maxima of σ_A, accuracy better than $\lambda/250$ was obtained. The absolute accuracy of the proposed technique was assessed using a single phase reconstruction, randomly selected from a set of performed measurements. Phase errors at the individual points of the image plane were evaluated with respect to an ideal planar surface. The standard deviation was evaluated by processing the phase errors over all pixels of the measured phase surface. Its value was determined as $\sigma = 0.028$ radians, providing the surface profile accuracy of $\lambda/225$ with the peak-to-valley given by $\lambda/43$.

In further experiment, practical applicability of the method was tested and an array of microlenses with parameters provided by the producer was used as a sample (Thorlabs, MLA300-14AR). The experimental results (Fig. 20) were compared with the nu-

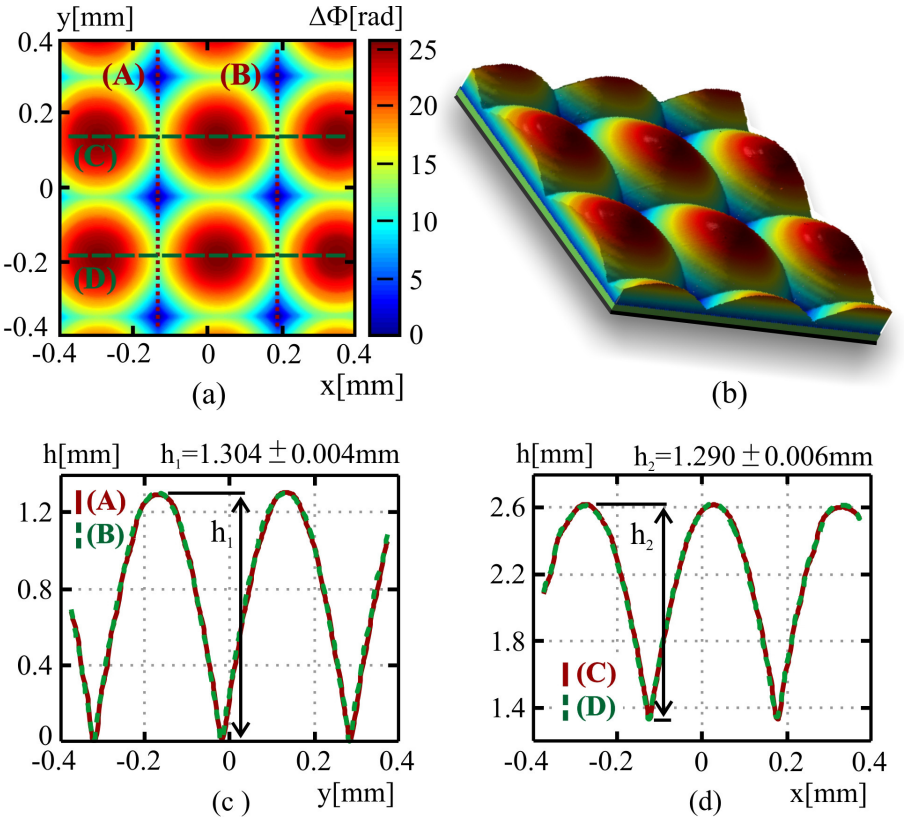

Figure 20: Phase reconstruction of the array of microlenses (Thorlabs, MLA 300-14 AR) [15]: (a) unwrapped phase with color representation of the phase levels, (b) 3D illustration of the unwrapped phase, (c) height profiles across the valleys of the microlenses (sections A and B), (d) height profiles across the tops of the microlenses (sections C and D) [15].

merical simulation carried out using the parameters given in the Thorlabs catalog. In the measured array, square plano-convex microlenses with the theoretical focal length $f = 18.6$ mm, the radius of curvature $r = 8.6$ mm and the pitch $p = 300$ μm were used. By means of r and p, the maximal height of the spherical cap along the diagonal of the array was calculated, $h = 2.616$ μm. The maximal height h is given by the sum of the spherical cap heights h_1 and h_2 evaluated along the sections A and C in Fig. 20a, $h = h_1 + h_2$. For the theoretical parameters, both heights take the same value, $h_1 = h_2 = 1.308$ μm. The surface topography obtained by the measurement (Figs. 20a and 20b) was evaluated in sections A, B (Fig. 20c) and C, D (Fig. 20d) taken across the valleys and the tops of the microlenses, respectively. In the statistical assessment of the experimental results, the microlenses available in the field of view of the MIO were used. Evaluating the experimental data, heights of the spherical caps in the sections A, B and C, D were determined as $h_1 = (1.304 \pm 0.004)$ μm and $h_2 = (1.290 \pm 0.006)$ μm, respectively. The pitch of the microlenses was measured, $p = (303.6 \pm 0.9)$ μm. By the best fitting of the experimental data, the radius of curvature of the microlenses $r = 8.68$ mm was determined, which is also close to the value given by the producer.

5.4. Multimodal microscope aided by spatial light modulation

In recent time, a great potential of the SLM aided imaging has been discovered both theoretically and experimentally. In the doctoral thesis, the universal system capable of altering different imaging modes has been developed, which can be advantageously implemented using an add-on module (AOM) connected to a standard optical microscope. The AOM enables unification of the individual imaging modes into the same optical path, resulting in a versatile SLM based multimodal microscope. The multimodal microscope was accepted as one of the main outputs of the project CDO supported by the TA CR.

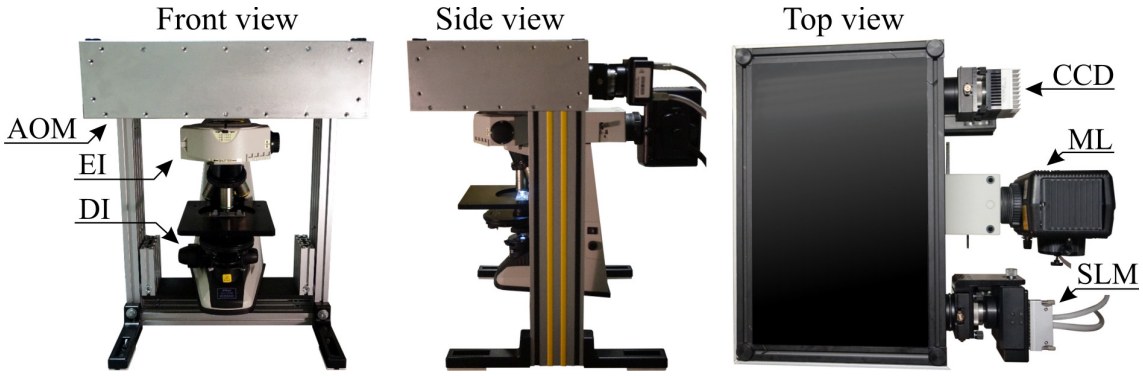

Figure 21: Photographs of the multimodal microscope aided by the spatial light modulation: AOM-add-on module; EI-episcopic illumination; DI-diascopic illumination; ML-mercury lamp.

Optical design of the multimodal microscope is based on the commercial upright microscope Nikon Eclipse E200. Using Nikon accessories, standard diascopic and episcopic imaging modes are available. Conditions needed for an optimal operation of the SLM were carefully considered in the design of the AOM. Connecting the AOM to the optical microscope, the SLM is placed at the Fourier plane, optically conjugate with the condenser diaphragm and the exit pupil of the MO, respectively. It provides a multitude of optical applications including optical filtration, shaping of special beams or advantageous beam splitting. Mechanical construction of the multimodal microscope was designed by Ing. Martin Antoš, Ph.D. Concept of the mechanics was prepared according to the optical design and its requirements were taken into account. In the mechanical construction, commercially available, customized and custom fabricated components were used, providing maximal mounting flexibility of both optical and mechanical elements. Photographs of multimodal microscope are presented in Figs. 21a-c.

5.4.1. Early experimental testing

Although the final completion of the multimodal microscope including control and monitoring functions is scheduled to 2017 within the TA CR project, the system has been functional since 2015. Its operation was examined in the doctoral thesis with the particular attention focused on testing of the compatibility between the AOM and the commercial microscope Nikon Eclipse E200.

In experiments, the bright-field imaging, Zernike phase contrast and dark-field imaging were implemented with the diascopic illumination (DI), while epifluorescence imaging was tested using the episcopic illumination (EI). Results obtained are presented in Figs. 22–24. A comparison of the bright-field and Zernike phase contrast imaging is performed in

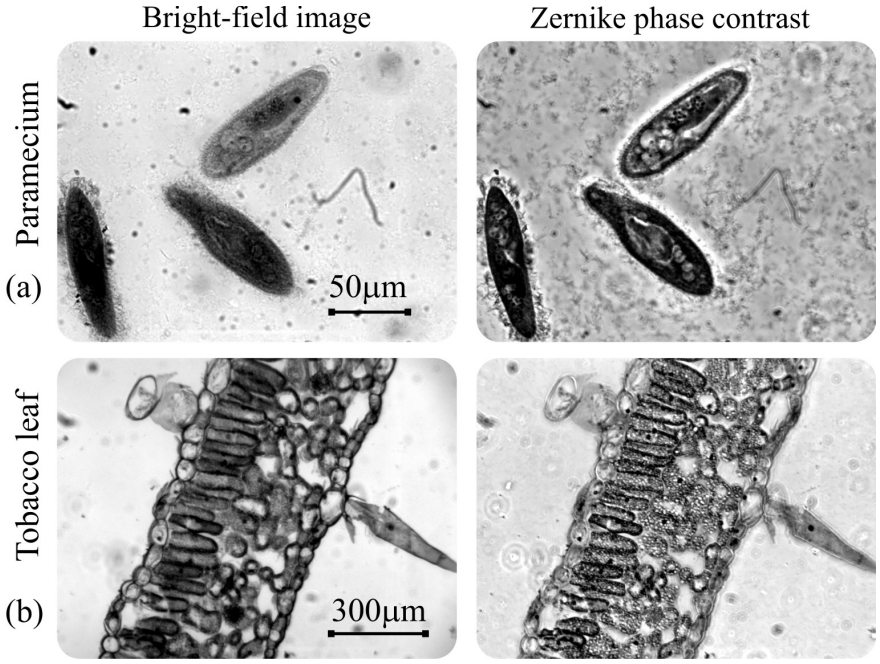

Figure 22: Experimental testing of Zernike phase contrast imaging in the multimodal microscope and its comparison with bright-field imaging using (a) paramecium and (b) tobacco leaf as samples.

Figs. 22a,b. Specimens of paramecium were used as a testing sample in Fig. 22a. Images obtained in both bright-field and Zernike phase contrast imaging modes were captured using the MO Nikon $20\times/NA = 0.5$ ($f_0 = 10$ mm). Contrary to the bright-field image, nucleus and vacuoles of paramecium are apparent in Zernike phase contrast. In Fig. 22b, the MO Nikon $10\times/NA = 0.3$, ($f_0 = 20$ mm) was utilized and a tobacco leaf used as a sample. Mesophyll cells including their inner structure are observable in Zernike phase contrast. Both dark-field and epifluorescence imaging was tested utilizing the MO Nikon $20\times$. During the dark-field imaging, a jasmine leaf was used as a sample and its amplitude transitions were successfully enhanced (Fig. 23). In the epifluorescence experiment, fluo-

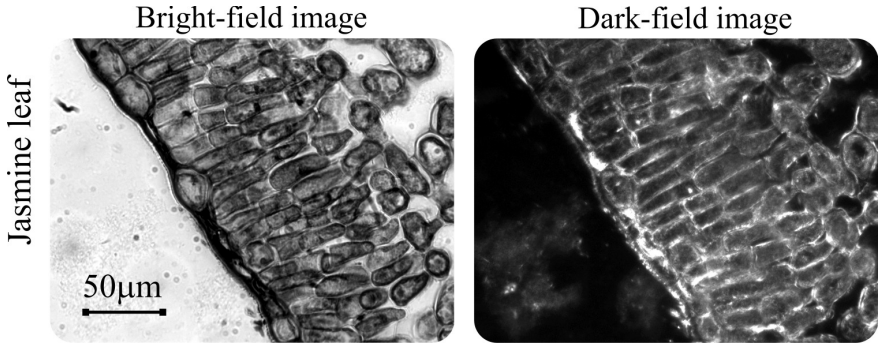

Figure 23: Experimental testing of dark-field imaging in the multimodal microscope and its comparison with bright-field imaging using jasmine leaf as a sample.

rescent microspheres (Invitrogen 1 μm in diameter) were utilized, providing a calibration of imaging system (Fig. 24a). In further experiment, cellulose molecules in fiber from a paper towel were excited and fluorescence image recorded (Fig. 24b).

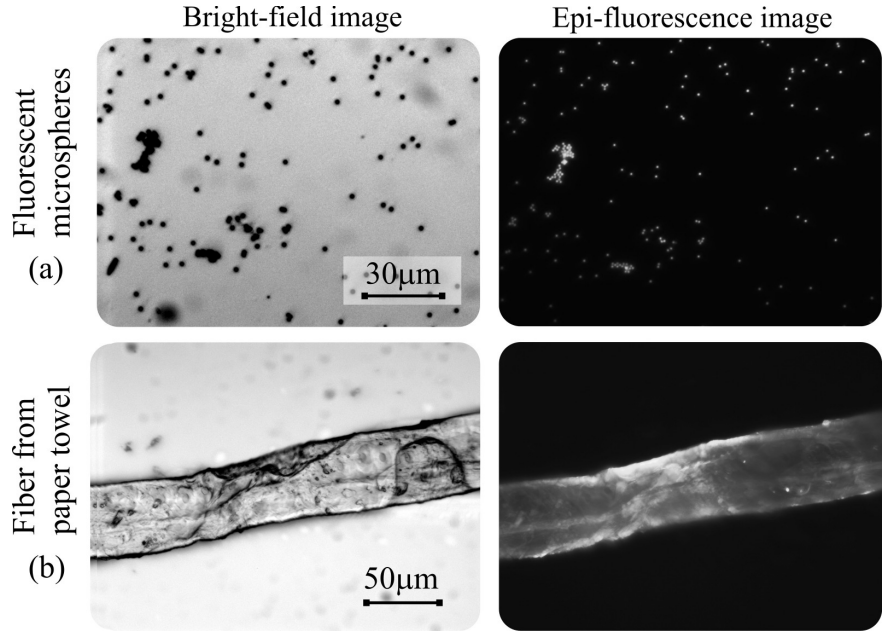

Figure 24: Experimental testing of epifluorescence imaging in the multimodal microscope and its comparison with bright-field imaging using (a) fluorescence microspheres and (b) fiber from paper towel as samples.

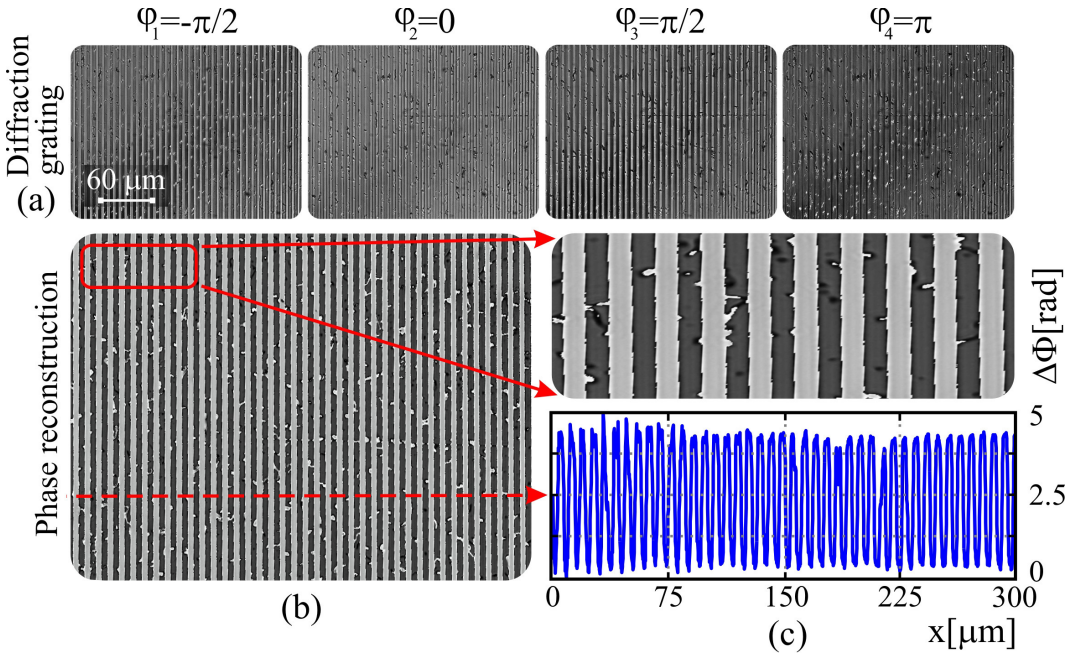

Figure 25: Demonstration of quantitative phase imaging in the multimodal microscope. (a) Zernike phase contrast images of diffraction grating with phase shifts $\varphi_j = (j-2)\pi/2, j = 1, 2, 3, 4$ imposed on light unaffected by the sample. (b) Quantitative phase reconstruction. (c) Enlarged subarea and cross section of quantitative phase reconstruction.

In advanced experiments, the imaging performance of the multimodal microscope was assessed, using the SLM based methods. During the advanced experimental testing, the methods examined throughout the doctoral thesis were implemented. Beyond the originally proposed methods, also some previously presented experiments on the SLM

imaging were successfully reproduced. Combining benefits of Zernike phase contrast and phase-shifting holography, the quantitative phase imaging is possible [46]. During the experimental testing of the quantitative phase imaging, the MO Nikon 20× was utilized and a phase diffraction grating used as a sample. The phase shifted Zernike images of the grating and its quantitative phase reconstruction are presented in Figs. 25a,b. In Fig. 25c, both enlarged subarea of the quantitative phase reconstruction and phase profile perpendicular to the grating grooves are shown. Evaluating measured data, the height of grating grooves $h = (335 \pm 7)$ nm was reconstructed. In order to assess obtained results, a reference measurement was performed applying technique of the CCHM [7–10]. During the measurement, the holographic microscope Q-Phase was used [47]. Deploying the reference technique, the similar height of grating grooves $h = (324 \pm 6)$ nm was obtained.

6. Conclusion

The doctoral thesis deals with the modern optical imaging methods based on advanced techniques of light shaping and digital signal processing. Throughout the doctoral thesis, principles of optical microscopy, digital holography and incoherent correlation imaging have been systematically studied and the imaging performance of the developed methods enhanced in experiments aided by modern SLM technologies and recent discoveries of singular optics. The research outcomes, presented in both scientific and applied parts of the doctoral thesis, were published in prestigious peer-reviewed journals and contributed to the current state of the art in monitored areas of optics. The results achieved enriched theoretical and experimental know-how available at the IPE BUT and created background for ongoing research activities.

The doctoral thesis is based on theoretical concepts arising from a systematic study of the latest discoveries in the relevant areas of optics, especially in singular, nondiffracting, digital and Fourier optics. The main conceptual aim of the doctoral thesis was to incorporate nontraditional states of light and special optical phenomena into imaging sciences, where they were previously rarely used. The main attention was focused on vortex and nondiffracting light fields and unique self-imaging effects arising from their interference. The theoretical results were validated in experiments carried out using the SLM as a basic experimental tool. The experiments were designed with regard to envisaged applications and their results were used for optimization, enhancement and usability evaluation of the developed methods. The overall significance and impact of the results of the doctoral thesis may be summarized as follows:

- Principles and experiments of the SLM aided imaging were reviewed and original concepts enriching the imaging sciences proposed. In this way, a comprehensive study on novel imaging technologies at the IPE BUT was created.

- Through the results of the doctoral thesis new research program was outlined and adopted at IPE BUT, which was successfully incorporated into the projects of basic and applied research supported by the GA CR and TA CR.

- Research within the doctoral thesis and the project funding provided theoretical and experimental background at the IPE BUT, enabling cutting-edge experiments on the SLM aided imaging.

- The particular results of the doctoral thesis were exploited in the design of the multimodal microscope, in which specific imaging modes have been incorporated including fluorescence correlation imaging, spiral imaging, Zernike phase contrast imaging, quantitative phase reconstruction and three-dimensional localization and tracking of microobjects. Utility model of the multimodal microscope was intended as one of the objectives of the TA CR project.

Abbreviations

AOM Add-On Module 28

CCD Charge-Coupled Device 2

CCHM Coherence Controlled Holographic Microscopy 1

CDO Center of Digital Optics 1

CGH Computer Generated Hologram 4

CR Correlation Record 12

DH PSF Double-Helix Point Spread Function 4

DI Diascopic Illumination 28

EI Episcopic Illumination 28

GA CR Grant Agency of the Czech Republic 1

IF Impact Factor 3

IPE BUT Institute of Physical Engineering Brno University of Technology 1

ISI Brno Institute of Scientific Instruments Brno 3

LCVR Liquid Crystal Variable Retarder 3

LED Light Emitting Diode 7

MIO Mirau Interference Objective 25

MO Microscope Objective 8

MTF Modulation Transfer Function 24

PSF Point Spread Function 2

QWP Quarter-Wave Plate 25

SCR Spiral Correlation Record 12

SLM Spatial Light Modulator 1

TA CR Technology Agency of the Czech Republic 1

UP Palacky University 1

References

[1] DURNIN, J. *Exact solutions for nondiffracting beams. I. The scalar theory.* J. Opt. Soc. Am. A **4**, 651–654, (1987).

[2] MONTGOMERY, W. D. *Self–Imaging Objects of Infinite Aperture.* J. Opt. Soc. Am. **57**, 772–775, (1967).

[3] PATORSKI, K. *The self–imaging phenomenon and its applications.* Progress in Optics **27**, E. Wolf, ed., North–Holland, Amsterdam, (1990).

[4] SOSKIN, M. S.; VASNETSOV, M.V. *Singular Optics.* Progress in Optics **42**, 219–276, (2001).

[5] BOUCHAL, P. *Bachelor thesis: Fresnelova nekoherentní korelační holografie (FINCH).* Brno: Brno University of Technology, Faculty of Mechanical Engineering, 1–41, (2010).

[6] BOUCHAL, P. *Diploma thesis: Fresnelova nekoherentní korelační holografie (FINCH).* Brno: Brno University of Technology, Faculty of Mechanical Engineering, 1–63, (2012).

[7] CHMELÍK, R.; SLABÝ, T.; KOLMAN, P.; DOSTÁL, Z.; ANTOŠ, M. *Interferometric system with spatial carrier frequency capable of imaging in polychromatic radiation.* Brno: Brno University of Technology, U.S. Patent 8526003 B2, (2013).

[8] KOLMAN, P.; CHMELÍK, R. *Coherence-controlled holographic microscope.* Opt. Exp. **18**, 21990–22003, (2010).

[9] SLABÝ, T.; KOLMAN, P.; DOSTÁL, Z.; ANTOŠ, M.; LOŠŤÁK, M.; CHMELÍK, R. *off-axis setup taking full advantage of incoherent illumination in coherence-controlled holographic microscope.* Opt. Exp. **21**, 14747–14762, (2013).

[10] LOŠŤÁK, M.; CHMELÍK, R.; SLABÁ, M.; SLABÝ, T. *Coherence-controlled holographic microscopy in diffuse media.* Opt. Exp, **22**, 4180–4195, (2014).

[11] BOUCHAL, P.; BOUCHAL, Z.; CHMELÍK, R. *Jednocestná nekoherentní korelační mikroskopie: metody, aplikace a výzkum v Centru digitální optiky TA ČR.* Jemná mechanika a optika, č. 6–7, 184–186, (2014).

[12] BOUCHAL, P.; BOUCHAL, Z. *Wide–field common–path incoherent correlation microscopy with a perfect overlapping of interfering beams.* JEOS:RP. **8**, 1–8, (2013).

[13] BOUCHAL, Z.; CHLUP, V.; ČELECHOVSKÝ, R.; BOUCHAL, P.; NISTOR, C. *Achromatic correction of diffractive dispersion in white light SLM imaging.* Opt. Exp **22**, 12046–12059, (2014).

[14] CHLUP, V.; BOUCHAL, Z.; BOUCHAL, P. *Afokální optický systém pro korekci barevné vady difraktivních zobrazovacích prvků.* Patent application and Utility model protection, (2015) (submitted).

[15] BOUCHAL, P.; ČELECHOVSKÝ, R.; BOUCHAL, Z. *Polarization sensitive phase-shifting Mirau interferometry using a liquid crystal variable retarder.* Opt. Lett. **40**, 4567-4570, (2015).

[16] BOUCHAL, P.; BOUCHAL, Z. *Concept of coherence aperture and pathways toward white light high–resolution correlation imaging.* New. J. Phys. **15**, 1–18, (2013).

[17] BARÁNEK, M.; BOUCHAL, P.; ŠILER, M.; BOUCHAL, Z. *Aberration resistant axial localization using a self–imaging of vortices.* Opt. Exp. **23**, 15316–15331, (2015).

[18] BOUCHAL, P.; KAPITÁN, J.; CHMELÍK, R.; BOUCHAL, Z. *Point spread function and two–point resolution in Fresnel incoherent correlation holography.* Opt. Exp. **19**, 15603–15620, (2011).

[19] BOUCHAL, P.; BOUCHAL, Z. *Non–iterative holographic axial localization using complex amplitude of diffraction–free vortices.* Opt. Exp. **22**, 30200–30216, (2014).

[20] BOUCHAL, P.; BOUCHAL, Z. *Selective edge enhancement in three–dimensional vortex imaging with incoherent light.* Opt. Lett. **37**, 2949–2951, (2012).

[21] BOUCHAL, P.; BOUCHAL, Z.; ČELECHOVSKÝ, R.; BARÁNEK, M. *Svazek1: Využití prostorového modulátoru světla v optickém zobrazení.* Research report, Center of Digital Optics TA CR, 1–60, (2013).

[22] BOUCHAL, Z.; BOUCHAL, P. *Optické víry aneb jak roztočit světlo.* Československý časopis pro fyziku, **65**, 351–354, (2016).

[23] Department of Optics, Palacky University Olomouc. Source: *http://www.ldo.optol.cz/cs/* [online]. 25.8.2015 (cited 2015–08–25).

[24] HOLOEYE Photonis AG. Source: *http://holoeye.com/spatial–light–modulators/* [online]. 13.4.2015 (cited 2015–04–13).

[25] Hamamatsu Photonics. Source: *http://www.hamamatsu.com/jp/en/4015.html* [online]. 13.4.2015 (cited 2015–04–13).

[26] Thorlabs Inc. Source: *http://www.thorlabs.de/NewGroupPage9.cfm?ObjectGroup_ID=6339* [online]. 27.8.2015 (cited 2015–08–27).

[27] ARCoptix. FT IR Spectrometers & Liquid Crystal Elements. Source:*http://www.arcoptix.com/variable_phase_retarder* [online]. 13.4.2015 (cited 2015–04–13).

[28] ROSEN, J.; BROOKER, G. *Digital spatially incoherent Fresnel holography.* Opt. Lett. **32**, 912–914, (2007).

[29] ROSEN, J.; BROOKER, G. *Fluorescence incoherent color holography.* Opt. Exp. **15**, 2244–2250, (2007).

[30] KATZ, B.; ROSEN, J.; KELNER, R.; BROOKER, G. *Enhanced resolution and throughput of Fresnel incoherent correlation holography (FINCH) using dual diffractive lenses on a spatial light modulator (SLM).* Opt. Exp. **20**, 9109–9121, (2012).

[31] BROOKER, G.; SIEGEL, N.; WANG, V.; ROSEN, J. *Optimal resolution in Fresnel incoherent correlation holographic fluorescence microscopy.* Opt. Exp. **19**, 5047–5062, (2011).

[32] YAMAGUCHI, I.; ZHANG, T. *Phase–shifting digital holography.* Opt. Lett. **22**, 1268–1270, (1997).

[33] ROSEN, J.; SIEGEL, N.; BROOKER, G. *Theoretical and experimental demonstration of resolution beyond the Rayleigh limit by FINCH fluorescence microscopic imaging.* Opt. Exp. **19**, 26249–26268, (2011).

[34] LAI, X.; ZENG, S.; LV, X.; YUAN, J.; FU, L. *Violation of the Lagrange invariant in an optical imaging system.* Opt. Lett. **38**, 1896–1898, (2013).

[35] ROSEN, J.; KELNER, R. *Modified Lagrange invariants and their role in determining transverse and axial imaging resolutions of self-interference incoherent holographic systems.* Opt. Exp. **22**, 29048–29066, (2014).

[36] LAI, X.; ZHAO, Y.; LV, X.; ZHOU, Z.; ZENG, S. *Fluorescence holography with improved signal to noise ratio by near image plane recording.* Opt. Lett. **37**, 2445–2447, (2012).

[37] BOUCHAL, P.; BOUCHAL, Z.; CHMELÍK, R. *Resolution Limits in Broadband Incoherent Correlation Imaging.* Digital Holography and 3D Imaging, OSA Technical Digest (online), paper DW2A.17, (2013).

[38] FÜRHAPTER, S.; JESACHER, A.; BERNET, S.; MARTE, M. *Spiral phase contrast imaging in microscopy.* Opt. Exp. **13**, 689–694, (2005).

[39] GREENGARD, A.; SCHECHNER, Y.; PIESTUN, R. *Depth from diffracted rotation.* Opt. Lett. **31**, 181–183, (2006).

[40] PAVANI, S.; PIESTUN, R. *High–efficiency rotating point spread functions.* Opt. Exp. **16**, 3484–3489, (2008).

[41] BARÁNEK, M.; BOUCHAL, Z. *Rotating vortex imaging implemented by a quantized spiral phase modulation.* JEOS–RP **8**, 1–8, (2013).

[42] PRASAD, S. *Rotating point spread function via pupil-phase engineering.* Opt. Lett. **38**, 585–587, (2013).

[43] ROIDER, C.; JESACHER, A.; BERNET, S.; MARTE, M. *Axial super–localisation using rotating point spread functions shaped by polarisation–dependent phase modulation.* Opt. Exp. **22**, 4029–4037, (2014).

[44] LEE, H.; SAHL, S.; LEW, M.; MOERNER, W. *The double–helix microscope super–resolves extended biological structures by localizing single blinking molecules in three dimensions with nanoscale precision.* Appl. Phys. Lett. **100**, 153701, (2012).

[45] BOUCHAL, P.; BOUCHAL, Z.; CHMELÍK, R. *Incoherent digital holography with axial localization by the rotating point spread function.* Imaging and Applied Optics, OSA Technical Digest (online), paper DM2B.4, (2014).

[46] WANG, Z.; MILLET, L.; MIR, M.; DING, H.; UNARUNOTAI, S.; ROGERS, J.; GILLETE, M.; POPESCU, G. *Spatial light interference microscopy (SLIM).* Opt. Exp. **19**, 1016–1026, (2011).

[47] TESCAN ORSAY HOLDING, a.s. Source: *http://www.tescan.com/en/products/q-phase/q-phase* [online]. 25.12.2015 (cited 2015–12–25).

CURRICULUM VITAE

PERSONAL DETAILS

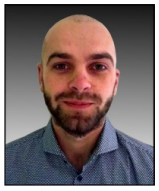

Name: Ing. Petr Bouchal
Address: Větrná 13, 750 02 Přerov VI–Újezdec, Czech Republic
Date of Birth: 1.4.1988
E-mail: Petr.Bouchal@ceitec.vutbr.cz
Nationality: Czech

EDUCATION

2012–present Doctoral studies, Faculty of Mechanical Engineering, BUT, Physical and Material Engineering

2010–2012 Ing., Master studies, Faculty of Mechanical Engineering, BUT, Physical Engineering and Nanotechnology

INTERNSHIPS

1.3.2011–1.9.2011 The University of Kent, School of Physical Sciences, Applied Optics Group

LIST OF PUBLICATIONS

[1] BOUCHAL, P.; KAPITÁN, J.; CHMELÍK, R.; BOUCHAL, Z. *Point spread function and two–point resolution in Fresnel incoherent correlation holography.* Opt. Exp. **19**, 15603–15620, (2011).

[2] BOUCHAL, P.; BOUCHAL, Z. *Selective edge enhancement in three–dimensional vortex imaging with incoherent light.* Opt. Lett. **37**, 2949–2951, (2012).

[3] BOUCHAL, P.; BRADU, A.; PODOLEANU, A. *Gabor fusion technique in a Talbot bands optical coherence tomography system.* Opt. Exp. **20**, 5368–5383, (2012).

[4] BOUCHAL, P.; BOUCHAL, Z. *Concept of coherence aperture and pathways toward white light high–resolution correlation imaging.* New. J. Phys. **15**, 1–18, (2013).

[5] BOUCHAL, P.; BOUCHAL, Z. *Wide–field common–path incoherent correlation microscopy with a perfect overlapping of interfering beams.* JEOS:RP. **8**, 1–8, (2013).

[6] BOUCHAL, Z.; CHLUP, V.; ČELECHOVSKÝ, R.; BOUCHAL, P.; NISTOR, C. *Achromatic correction of diffractive dispersion in white light SLM imaging.* Opt. Exp **22**, 12046–12059, (2014).

[7] BOUCHAL, P.; BOUCHAL, Z. *Non–iterative holographic axial localization using complex amplitude of diffraction–free vortices.* Opt. Exp. **22**, 30200–30216, (2014).

[8] BOUCHAL, P.; BOUCHAL, Z.; CHMELÍK, R. *Jednocestná nekoherentní korelační mikroskopie: metody, aplikace a výzkum v Centru digitální optiky TA ČR.* Jemná mechanika a optika, č. 6–7, 184–186, (2014).

[9] BARÁNEK, M.; BOUCHAL, P.; ŠILER, M.; BOUCHAL, Z. *Aberration resistant axial localization using a self–imaging of vortices.* Opt. Exp. **23**, 15316–15331, (2015).

[10] BOUCHAL, P.; ČELECHOVSKÝ, R.; BOUCHAL, Z. *Polarization sensitive phase–shifting Mirau interferometry using a liquid crystal variable retarder.* Opt. Lett. **40**, 4567–4570, (2015).

[11] BOUCHAL, Z.; BOUCHAL, P. *Optické víry aneb jak roztočit světlo.* Československý časopis pro fyziku, **65**, 351–354, (2016).

CONFERENCE PROCEEDINGS

[1] BRADU, A.; BOUCHAL, P.; PODOLEANU, A. *Enhancement of the signal-to-noise ratio at depths in Fourier domain optical coherence tomography.* In Proc. SPIE 8213, 1–5, (2012).

[2] BRADU, A.; MARQUES, M.; BOUCHAL, P.; PODOLEANU, A. *Combining Gabor and Talbot bands techniques to enhance the sensitivity with depth in Fourier domain optical coherence tomography.* In Proc. SPIE 8571, 1–6, (2013).

[3] BOUCHAL, P.; BOUCHAL, Z.; CHMELÍK, R. *Resolution Limits in Broadband Incoherent Correlation Imaging.* Digital Holography and 3D Imaging, OSA Technical Digest (online), paper DW2A.17, (2013)–poster presented by BOUCHAL, P.

[4] BOUCHAL, P.; BOUCHAL, Z.; CHMELÍK, R. *Incoherent digital holography with axial localization by the rotating point spread function.* Imaging and Applied Optics, OSA Technical Digest (online), paper DM2B.4, (2014)–oral presentation by BOUCHAL, P.

[5] BARÁNEK, M.; BOUCHAL, P.; BOUCHAL, Z. *Self-imaging of optical vortices for 3D localization and wavefront assessment.* Digital Holography and Three–Dimensional Imaging, OSA Technical Digest (online), paper DW2A. 12, (2015).